

The mesoscale sediment transport due to technical activities in the deep sea

Jacek A. Jankowski and Werner Zielke ¹

Institut für Strömungsmechanik und Elektronisches Rechnen im Bauwesen,
Universität Hannover, Appelstraße 1, 30167 Hannover, Germany

Abstract

This paper presents a mesoscale model for sediment transport in the deep sea resulting from technical activities such as manganese nodule mining. The model includes the temporal variability of ambient currents, the modification of the water density due to suspended sediments (density driven flow), bottom boundary layer effects, and the influence of flocculation on the sediment settling velocity. It yields the three-dimensional sediment concentration and the bottom blanketing for time periods of up to a few weeks in areas of up to a few hundred square kilometers. The model also allows simulation of the mobilization, sorption and the transport of heavy metals. Two applications are presented. One of them treats the sediment transport during the National Oceanic and Atmospheric Administration Benthic Impact Experiment. The other is concerned with dispersion of heavy metals, including the interaction with suspended sediment in the Disturbance and Recolonization Experiment Experimental Area. The model is highly sophisticated with regard to the processes and numerical methods. Nevertheless, a final conclusion concerning the quantification of its prognostic capability for industrial scale operations cannot presently be drawn because of the lack of complete and coherent data sets.

Key words:

Mesoscale sediment transport modeling, environmental impact assessment, SE Pacific.

Introduction

The main aim of the modeling presented in this paper is the assessment of the environmental impacts caused by various human activities, in particular the distribution of pollutants and effluents. In the case of deep-sea mining (Oebius et al., 2001), the modeling is used to forecast the fate of discharged material plumes and

¹ Corresponding author, e-mail: zielke@hydromech.uni-hannover.de

seafloor blanketing caused by settling particles. The parameters to be considered are those describing the exposure of marine organisms to large amounts of various particles (sediments, ore particles, biota) and other effluents (e.g. heavy metals) in concentrations and deposition fluxes exceeding ambient oceanic ones. Basically, it is necessary to estimate how long the mining plume persists before it eventually dilutes and reaches the approximate ambient concentration level or settles to the bottom and the resulting new sediment coverage in the affected areas.

The prediction of environmental impacts caused by deep-sea mining cannot be formulated without realistic assumptions concerning the deposits and the applied technology. Of greatest interest to the deep-sea mining industry are manganese nodules, which appear in form of flat horizontal fields on the ocean floor in depths of about 4000–6000 m. At present industry favors nodule recovery by a mining system consisting of a mining platform or ship at the surface and a remotely-controlled and self-propelled mining device (miner) operating at the bottom and connected to a riser for nodule transport (Oebius et al., 2001). With this technique, the largest impacts can be expected in the reach of the miner. The greatest sediment discharge appears in the bottom zone (90% or more), and a minor one originates from the mining vessel.

This paper focuses on the mesoscale modeling of dispersion and re-sedimentation of the near-bottom plumes. The time scales involved vary from hours to weeks, with the spatial resolution ranging from 100 m to 1 km. At this scale a considerable range of physical phenomena influencing the sediment transport in the benthic boundary layer must be taken into account. After an overall model description and a thorough discussion of critical modeling aspects, two applications will be presented: Sediment transport during the National Oceanic and Atmospheric Administration (NOAA) Benthic Impact Experiment and dispersion of heavy metals in the Disturbance and Recolonization Experiment (DISCOL) Experimental Area, including interaction with suspended sediment.

A short review of existing models and their data support

The models require field data, which are assimilated in order to formulate basic assumptions, treated as input data to operate the models or used for verification and validation. It is clear that the predictive quality depends strongly on the model-oriented data collection. Comparative studies made by the authors (Jankowski and Zielke, 1997) reveal that from the point of view of numerical modeling, the experiments for quantifying of model parameters are critical for the model accuracy and reliability. Therefore, despite various available oceanographic data, the specific field experiments strongly influence the modeling applications.

In the 1970s, during the Deep Ocean Mining Environmental Study (DOMES) project,

two successful and so far unique mining tests by Ocean Mining Inc. (OMI) and by Ocean Mining Associates (OMA) were monitored (Ozturgut et al., 1981; Lavelle et al., 1982). The impacts were produced by prototype mining devices, but the nodule recovery rate was about one order of magnitude lower than during planned commercial production. Models were developed to describe the bottom plume (Lavelle et al., 1981b) and the surface discharge, based on an analytical solution of the sediment transport equation in a uniform velocity field. The models were first applied to estimate sediment transport parameters, which were not observable, and then run in a prognostic mode. A few years later, Lavelle reanalyzed the problem using a two-dimensional numerical finite-difference model in order to include the effects of the bottom boundary layer, particle scavenging by marine snow, and new settling velocity laboratory analyses (Lavelle, 1987; Ozturgut and Lavelle, 1986).

In the 1980s, due to the fading interest of industry, there was no chance to improve the data obtained during mining tests. Therefore, post-DOMES experiments are characterized by the fact that the bottom disturbance and sediment resuspension were produced in a way similar to the action of real miners. During previous mining tests, efforts were made to monitor not only the redeposition at the bottom but also the plume in its various developmental stages. The later experiments, such as DISCOL (Thiel and Forschungsverbund Tiefsee-Umweltschutz, 2001), NOAA Benthic Impact Experiment (BIE) (Trueblood, 1993), Japan Deep Sea Impact Experiment (JET) (Fukushima, 1995), etc., concentrated on the bottom destruction and blanketing in the near field while the plume was neglected or inadequately observed (Jankowski and Zielke, 1997). Although the newer field experiments were not purposefully designed for the model-oriented data collection, almost all of them were accompanied by modeling.

Within the *Tiefsee-Umweltschutz* (TUSCH) group, using mainly data from their own DISCOL experiment (Thiel and Forschungsverbund Tiefsee-Umweltschutz, 2001), a three-dimensional, finite element, mesoscale model (Jankowski et al., 1996; Jankowski and Zielke, 1995) and a large-scale model with finite-differences (Zielke et al., 1995; Segschneider and Sündermann, 1997) were developed (Rolinski et al., 2001). The models profit mainly from the measurements accompanying the experiments and subsequent observations of recolonization by deep-sea organisms, the current measurements (Klein, 1993; 1996), the investigations of the bottom sediment properties (Becker et al., 2001; Grupe et al., 2001; Oebius et al., 2001), the overall oceanographic characteristics (Schriever, 1995; Schriever et al., 1996), and the heavy metal measurements (Koschinsky et al., 1997). The TUSCH modeling efforts concentrate on parameter sensitivity studies and scenario computations.

A Japanese research group (Taguchi et al., 1995; Nakata et al., 1997) developed a three-dimensional, finite-difference model applied to the JET and NOAA BIE experiments in the near field. Their characteristic approach is based on the fact that current measurements are incorporated directly into the model, yielding the velocity field. For model verification the re-sedimentation data from comparatively small

areas were used, and the effective settling velocity was compared to laboratory values.

As can be seen, most of the developed models are strictly connected with particular experimental activities. They differ greatly in the basic assumptions, the time and space scales, and the physical phenomena considered. The early models were specifically developed for the deep sea discharges, while the latest ones are adjustments of generic and complex models. There is an increasing tendency to include all relevant physical phenomena.

A mesoscale model for deep sea mining discharges

Conceptual model

The model developed by the authors concentrates on the time scales and areas where a considerable impact of the generated plumes is expected. The primary effort is to simulate the sediment transport under influence of time-variable mesoscale currents. The time and space resolution of this model allows the description of the plume spreading near the discharge site, starting when the ambient current begins to dominate the plume transport, i.e., after the first phase of dispersion by the eddies in the wake of the machine and after the subsequent gravity current action in the direct vicinity of the source. In order to take the movements of the miner into account, the spatial resolution is about 100 m, increasing to about 1 km away from the source. The upper time scale limit is defined by the range of the hydrodynamic processes described by the model. The model reproduces typical mesoscale hydrodynamic processes such as inertial oscillations, tides, and diurnal variations superimposed on a stable geostrophic component. It can be applied to transport for a period of time up to a few days with a resolution of about 10 minutes. The small scale processes are considered by diffusion coefficients.

Because of the size and location of the mining areas, a mesoscale model with open boundaries has been developed. Since the major discharges will take place in the bottom boundary layer, the modeling concentrates on this part of the water column. The model takes into account all of the relevant physical phenomena in the deepest ocean zone and yields results that describe the time-dependent, three-dimensional concentration fields, including the amount of redeposition and the plume residence time. In principle, the model consists of two modules dealing with hydrodynamics and transport of sediment and/or other effluents.

A three-dimensional hydrodynamic model

The mathematical modeling of the hydrodynamics is based on the theory for incompressible, turbulent free surface flows for geophysical applications. A description of the model is already provided in (Jankowski et al., 1996; Jankowski and Zielke, 1995) and therefore, only the most important features and new developments are described.

The equations for the primitive hydrodynamic variables are formulated in the Cartesian coordinate system (x is directed eastward, y northward, and z is positive upward) so that the model is applicable to horizontal motion scales at least one order of magnitude lower than the radius of the earth. The momentum conservation equations for the unknown three-dimensional velocity field $\mathbf{u} = (u, v, w)$ assume the Reynolds-averaged form of the Navier-Stokes equations:

$$\frac{\partial \mathbf{u}}{\partial t} + \mathbf{u} \cdot \nabla \mathbf{u} + 2\boldsymbol{\Omega} \times \mathbf{u} = -\frac{1}{\rho_0} \nabla p + \frac{\rho}{\rho_0} \mathbf{g} + \nabla \cdot (\nu \nabla \mathbf{u}) \quad (1)$$

where p represents the pressure, t time, $\boldsymbol{\Omega}$ is the earth's angular speed and \mathbf{g} the acceleration of gravity. The Boussinesq approximation is applied in which the density variations are taken into account in terms of buoyancy forces and neglected where the density appears as a parameter describing fluid inertia. The influence of the temperature and salinity variability on the stratification in the mixed deep-sea bottom boundary layer is assumed to be negligible. As a consequence of the incompressibility ($\nabla \cdot \mathbf{u} = 0$), it is assumed that the fluid volume is conserved while the density (and so the mass) changes freely as a function of sediment concentration only.

The roughness coefficient is computed by assuming the existence of a logarithmic velocity profile in the lowest part of the bottom boundary layer. The vertical turbulent eddy viscosity ν_z and turbulent diffusion coefficients for transported sediment are described by a mixing-length model with damping functions (dependent on the Richardson number) so that the stratification dampens the vertical mixing. The thickness of the bottom boundary layer in deep water is controlled by one parameter δ (Mofjeld and Lavelle, 1984). The logarithmic layer, where the velocity is constant in direction and increases logarithmically in magnitude, is assumed to occupy the lowest part of the bottom boundary layer (approximately between the bottom and 0.2δ). Consequently, the logarithmic layer is situated in the zone where the mixing length increases linearly. The Ekman layer occupies the remaining part of the bottom boundary layer above the logarithmic layer.

The numerical solution method is based on the well-validated TELEMAC3D code (Galland et al., 1991; Jankowski, 1999). The decoupled algorithm is based on the fractional step (operator-splitting) technique. Here the solution is obtained in sub-

sequent stages, each having well-defined mathematical properties so that the most adequate methods for a given differential operator type can be used. The majority of these steps uses the finite element method for space discretization (e.g. to treat the diffusion part) while for the advection, various other schemes, such as those based on the method of characteristics, are available. The finite difference method is applied for the time discretization and the computational domain variability is taken into account by a standard σ -mesh structure which is well suited to most geophysical applications.

A new feature of the model, compared to the one already described (Jankowski et al., 1996), is a non-hydrostatic option. In its original form, the model solves the three-dimensional shallow-water equations, i.e. it uses the hydrostatic approximation. This is based on the assumption that the vertical acceleration dw/dt can be neglected when the horizontal motion scales are large as compared to the vertical ones. In the non-hydrostatic version, no intrinsic assumptions are made as to the vertical acceleration, and the Navier-Stokes equations (1) are treated in their fully three-dimensional, original form (Jankowski, 1999). The vertical acceleration is taken into account by decomposing global pressure p into its hydrostatic p_H (i.e. barotropic as well as baroclinic) and hydrodynamic π components:

$$p = p_H + \pi \quad (2)$$

The solution algorithm follows the fractional step method, where in the first two stages (advection, diffusion), an intermediate solution for the velocity $\tilde{\mathbf{u}}$ is obtained by solving the momentum equation without taking hydrodynamic pressure gradients into consideration:

$$\frac{\tilde{\mathbf{u}} - \mathbf{u}^n}{\Delta t} + \mathbf{u} \cdot \nabla \mathbf{u} = -\frac{1}{\rho_0} \nabla p_H^n + \nabla \cdot (\nu \nabla \mathbf{u}) - 2\boldsymbol{\Omega} \times \mathbf{u} \quad (3)$$

where the hydrostatic part is computed explicitly from the free surface elevation and density field. In general, $\tilde{\mathbf{u}}$ is not divergence-free. The hydrodynamic pressure is found from the pressure Poisson equation:

$$\nabla^2 \pi = \frac{\rho_0}{\Delta t} \nabla \cdot \tilde{\mathbf{u}} \quad (4)$$

The final velocity is obtained under the assumption of incompressibility ($\nabla \cdot \mathbf{u}^{n+1} = 0$) from the projection of the intermediate result $\tilde{\mathbf{u}}$:

$$\mathbf{u}^{n+1} = \tilde{\mathbf{u}} - \frac{\Delta t}{\rho_0} \nabla \pi \quad (5)$$

Using the resulting final velocity, the position of the free surface can be found. For deep-sea applications, it is obtained from the conservative formulation of the free-

surface equation, which is the vertically integrated continuity equation with both kinematic and bottom impermeability boundary conditions taken into consideration:

$$\frac{\partial S}{\partial t} = -\frac{\partial}{\partial x} \int_{-B}^S u dz - \frac{\partial}{\partial y} \int_{-B}^S v dz \quad (6)$$

Model forcing

The main problem regarding the simulation of the hydrodynamics is to obtain the mesoscale flow variability in the relatively small domain with all boundaries open. Due to this fact, an approach based on measurements has been chosen. In the model, currents above the bottom boundary layer are obtained by applying prescribed *barotropic* pressure gradients taken from Fourier analysis of the current measurements during the experiment (Jankowski et al., 1996). Their variations produce a current scenario very similar to the original current. The bottom boundary layer forms freely in a natural way below the geostrophic region.

In order to produce typical current scenarios, current measurements in appropriate resolution are needed to detect and quantify the most important hydrodynamic phenomena (tides, inertial waves, eddies, bottom boundary layer). Special attention must be paid to the characterization of the turbulent bottom boundary layer (bottom roughness, velocity profile). The turbulent viscosities and diffusivities with their spatial and temporal variability also are obtained from the current measurements using statistical methods. The measurements of salinity, temperature, and turbidity profiles provide the ambient, normal particle concentrations and density fields. In order to take into account the topographic influences on the currents, the bathymetry of the area in sufficient resolution for the given model scale is needed.

Sediment transport

The transport processes are modeled by solving transport equations for the suspended sediment and/or passive effluents with appropriate initial and boundary conditions (McLean, 1985). From the mathematical point of view, the transported substances can be divided into active and passive tracers that do or do not influence the fluid density. For suspended transport modeling, the settling velocity of the sediment must be taken into account.

The transport equation for sediment is:

$$\begin{aligned} \frac{\partial c}{\partial t} + u \frac{\partial c}{\partial x} + v \frac{\partial c}{\partial y} + w \frac{\partial c}{\partial z} + \frac{\partial(w_s c)}{\partial z} &= \frac{\partial}{\partial x} \left(v_{xc} \frac{\partial c}{\partial x} \right) \\ &+ \frac{\partial}{\partial y} \left(v_{yc} \frac{\partial c}{\partial y} \right) + \frac{\partial}{\partial z} \left(v_{zc} \frac{\partial c}{\partial z} \right) + q_c + q_s \end{aligned} \quad (7)$$

where c is the dry mass sediment concentration, (u, v, w) the velocity field, w_s is the settling velocity, v_{ic} denotes the sediment eddy diffusivity, q_c is a source term describing the discharge, and q_s represents the scavenging rate by alien particles (as marine snow). The value of the settling velocity in the assumed coordinate system is negative. The reported maximum sediment concentrations in the bottom plume, in the range of 10 g/l (Lavelle et al., 1981b), are sufficiently small so that the volume fraction occupied by the sediment can be neglected.

The boundary conditions of the Equation (7) are described as follows. The net sediment flux at the surface (or at an upper boundary of the model) is zero:

$$\left[w_s c - v_{zc} \frac{\partial c}{\partial z} \right]_{\text{surf}} = 0 \quad (8)$$

Erosion and sedimentation at the sediment-water interface are usually taken as the functions of the bed shear stress τ_b , the critical shear stress of deposition τ_{cd} , and the critical shear stress of erosion τ_{ce} (Krone, 1962). If the bed shear stress exceeds the critical deposition shear stress, a particle settled on the bed will immediately be resuspended. If the bed shear stress is less than τ_{ce} , no erosion will occur. Consequently, the bottom boundary condition is formulated as follows:

$$\left[w_s c - v_{zc} \frac{\partial c}{\partial z} \right]_{\text{bot}} = w_s c_b f_d + M_{\text{res}} f_e \quad (9)$$

where the probabilities for deposition f_d and erosion f_e are given by (Krone, 1962):

$$f_d = \begin{cases} 0 & \tau_b \geq \tau_{cd} \\ (1 - \tau_b / \tau_{cd}) & \tau_b < \tau_{cd} \end{cases} \quad (10)$$

$$f_e = \begin{cases} 0 & \tau_b < \tau_{ce} \\ (\tau_b / \tau_{ce} - 1) & \tau_b \geq \tau_{ce} \end{cases} \quad (11)$$

The resuspension rate M_{res} and the critical stresses τ_{ce} and τ_{de} must be obtained from empirical formulations. Erosion and deposition processes can be described without difficulty in the low-energetic boundary layer, typical for the regions of

deep-sea mining. The small velocity magnitudes detected by long-term measurements (Bischoff et al., 1979; Klein, 1993) allow the assumptions that no erosion occurs and that each plume particle that reaches the bottom deposits. In this case $f_e = 0$ and $f_d = 1$. If mining takes place in regions of stronger currents, the formal description of erosion and deposition processes must be introduced. Very little is known about these parameters for the deep-sea sediments (McCave and Gross, 1991).

The current velocity field is given by the hydrodynamic module of the model. However, the presence of the discharged particulate mass in higher concentration influences the ambient current. The suspended particles change the local fluid density, causing stratification and buoyancy effects as density (gravity) currents. The intensity of these phenomena depends mainly on the magnitude of the density difference between the discharge and the surrounding fluid. The persistence of buoyancy effects depends on the mixing rate, which diminishes flow-driving density gradients. The reduced vertical mixing due to the stable stratification has an important influence on the concentration distribution in the first stages of plume transport.

In the model, it is assumed that the suspended sediment interacts with the current by influencing the local fluid density according to the equation of state:

$$\rho(S, T, c) = \rho(S, T) + \frac{\rho_{\text{sed}} - \rho(S, T)}{\rho_{\text{sed}}} \cdot c \quad (12)$$

The stratification caused by the suspended sediment dampens the vertical mixing according to the mixing length turbulence model mentioned above.

The *sediment settling velocity in situ* w_s is the most complex parameter and must be discussed in detail. The particle size distribution of the sediments from the mining areas (Table 1) shows that most of the particles have diameters smaller than $60\mu\text{m}$ so that the cohesive forces between the particles cannot be neglected (McCave, 1984; Klein, 1993). The plume particles interact with each other, building aggregates (flocculation) and breaking up. Laboratory experiments using sediments from the equatorial Pacific mining areas have shown that flocculation effects are significant in the plumes at concentrations above 0.1 g/l (Ozturgut and Lavelle, 1986). These higher concentrations, under which flocculation effects are stronger, are found in the direct vicinity of the source and may reach from 1 g/l to 10 g/l . Settling velocities for the plume particles range from 10^{-3} m/s to 10^{-7} m/s , which means that this sediment transport parameter requires special attention. In the sediment transport model, the settling velocity can be treated using the following methods:

- (1) it is assumed that the settling velocity is constant in time and space (non-cohesive case);
- (2) the particle diameter spectrum is distributed into a number of non-interacting

- sediment classes characterized by different settling velocities (non-cohesive case);
- (3) an empirical approach is used to deal with flocculation and break-up processes, resulting in a formula for the mean settling velocity (cohesive case);
 - (4) a number of sediment classes is chosen and interactions among them are accounted for (cohesive case).

In order to apply the non-cohesive cases (1) or (2), it is assumed that the information provided by the particle diameter and density distributions is sufficient to obtain the settling velocity. The mean settling velocity w_{sm} of the composite sediment spectrum can be calculated from:

$$w_{sm} = \frac{\sum_i w_{si} c_i}{\sum_i c_i} \quad (13)$$

where c_i are the dry mass concentrations of the fraction characterized by the diameter d_i and settling velocity w_{si} . In case (2), the different sediment classes settle independently and the mean settling velocity diminishes with the age of the plume as the larger particles settle out. In case (1), the settling velocity remains constant in time. For a given time scale of transport, it is possible to calibrate this constant velocity to formulate conservative forecasts comparable to those obtained with a number of sediment classes (Jankowski and Zielke, 1995).

In order to take into account the cohesive sediment properties influencing the mean sediment settling velocity, the empirical formulations, case (3), are available. The processes of aggregation and break-up of particles are parameterized using suspended sediment concentration and turbulent shear. According to this parameterization, the break-up phenomena are insignificant in the low-energetic deep sea bottom boundary layer. Differential settling dominates other flocculation mechanisms as Brownian motion and turbulent shear (McCave, 1984). In this case, an empirical model is appropriate in which the settling velocity is a function of the sediment concentration only (Jankowski et al., 1996). Therefore, the possible flocculation effects may only accelerate the deposition. Unfortunately, data describing the cohesive properties of the deep-sea sediments *in situ* presently are too scarce to allow the application of this formulation in a non-speculative way (McCave and Gross, 1991). It is difficult, but feasible, to describe sediment settling using a flocculation model based on a spectrum of interacting (i.e. cohesive) sediment classes, case (4), (Hill and Nowell, 1995). The most serious problems encountered are uncertainties in interaction rates, especially in a concentration model. Because of the difficulties mentioned above, the approaches (3-4) were not followed. Since it is very difficult to measure the parameters describing the settling velocity *in situ* (McCave and Gross, 1991), even for the seemingly simplified non-cohesive cases (1-2), most estimations are based on laboratory experiments.

Due to the fact that the flocculation may be insignificant at low concentrations away

from the source, scavenging is the only mechanism that may diminish the particle concentration. The scavenging rate q_s can be found by observing the vertical flux of the ambient particles appearing naturally in the ocean, as marine snow. These large, amorphous particles sweep large ranges of the water column, collecting finer particles underway and transporting them downwards. If the mining plume drifts in areas swept by these particles, scavenging may be an effective agent in removal of the diluted plumes if they consist of slowly settling fine particles (Lavelle, 1987; Jankowski et al., 1996).

Although the resuspension experiments give a chance to estimate the settling velocity *in situ* and to clear the uncertainties concerning the stratification effects and density currents, these aspects have not been addressed properly (Jankowski and Zielke, 1997). There were no attempts to clear the uncertainties concerning the diluted plumes drifting at a distance from the source.

Source quantification

For proper formulation of the source term $q_c(x, y, z, t)$ of the transport equation, the discharge rate and the form in which it takes place must be carefully quantified taking into consideration the type of mining devices, sediment properties, and mining area characteristics (Ozturgut et al., 1981). Additionally, some generalization must be made with regard to the discharge, according to the model resolution in time and space. Unfortunately, no measurements concerning industrial devices in action are available.

The mass available for discharge in the upper layer of the bottom sediments, which is disturbed by the devices, defines the maximum discharge rates. Worst-case estimates are usually formulated assuming this amount, but they cannot be free from assumptions concerning the devices. The initial concentration and density of the discharge are important for characterization of density effects in the first stages of sediment transport.

The estimates presented by (Oebius et al., 2001) yield discharge rates approaching 90 kg/s and concentrations up to 1.6 g/l in the wake of the industrial mining device with a 6 m wide collector on a carrier moving with a speed of 1 m/s. During the Benthic Impact Experiment, the sediment was resuspended by a special device, a *benthic disturber* (Trueblood, 1993). Its mean discharge is reported to be about 4 kg/s, with maximum concentration in the origin of the jet-like discharge locally reaching 30 g/l. The towing velocity is about 0.5 m/s. In all cases the speed of the device is greater than the ambient current.

The observations of the re-sedimentation pattern of the bottom plume during the mining tests and BIE experiments allow the supposition that density-driven flow plays a role in the first transport stages of the discharged sediment. The time and

space scales associated with these flows remain unmeasured, but intensive re-sedimentation is found up to 100 m or more *upstream* of the collector tracks. This has been interpreted as the consequence of density flows (Lavelle et al., 1981b; Nakata et al., 1997; Ozturgut et al., 1997).

Numerical studies in the vicinity of a source show that gravitational effects generate near-bottom, flat distribution of the bottom plume in the initial stages after discharge, causing an additional settling effect of the plume (Jankowski et al., 1994). After the initial phase of dispersion by the eddies in the wake of the machine and the subsequent gravitational collapse in the direct vicinity of the source, the concentrations diminish and the ambient current prevails as the main transport mechanism. How much resettles immediately to the bottom, and how much remains in the water column and is available for further dispersion by ambient currents, is questionable (Becker et al., 2001). Therefore, some assumptions must be made for the mathematical formulation of the source term q_c for the mesoscale transport.

The mining devices most probably will move in alternate directions on the bottom with a speed of 0.5-1 m/s following a linear path. They will cover distances of up to a few km from the mining ship. The miner with parameters mentioned above is able to mine an area of about 0.5 to 1 km² daily, in a form of a prolonged rectangle. The long-term economic considerations would require that the area is mined as effectively as possible without leaving larger patches of untouched nodule fields. For navigational reasons, the tracks will probably be oriented accordingly to the prevailing current. This kind of mining discharge can be mathematically idealized for modeling purposes as a mass source moving in an oscillatory way in a relatively confined area (Jankowski et al., 1996). During the experiments using the *benthic disturber*, a similar pattern has been followed.

Modeling of the NOAA Benthic Impact Experiment

The data collected during the NOAA BIE experiment can be used to validate and discuss some features of the mesoscale model. The area covered by the data sampling is relatively small and the transport scales indicate that one has to deal with an almost near-field approach in this case.

General description

A new experimental approach was initiated in 1991 by NOAA (USA) in cooperation with the Central Marine Geological and Geophysical Expedition (CGGE) of Russia in the Clarion-Clipperton Fracture Zone (CCFZ) of the Pacific Ocean. The intention of the Benthic Impact Experiment (BIE) was to produce sediment

resuspension and subsequent deposition in an experimental area in order to obtain sediment burial of organisms and food resource dilution (Ozturgut et al., 1997). The action of a miner was simulated using a special device, a benthic disturber (Deep-Sea Sediment Resuspension System, DSSRS) (Brockett and Richards, 1994; Trueblood, 1993). The towed disturber is designed to liquify, lift and discharge a slurry of sediment a few meters above the bottom and to blanket an area of the sea floor in a manner which can be expected during mining activities. As in DISCOL, no nodules were removed from the bottom, but the experimental setting allowed a clear separation of the areas affected only by the deposition from the areas where the bottom structure was disturbed directly by the device sleds. The disturber was towed 49 times along a path of 3300 m length, producing a 150 m wide directly affected area. The tracks were situated perpendicularly to the predominant current direction. As a result, ca. 1450 t dry weight sediment was resuspended and a deposition with gradual reduction of the thickness at increasing distance from the tracks, ranging from 10 to 1 mm, was achieved in an area of about 2 km² (Trueblood, 1993).

For measuring the extent of the deposition, 18 sediment traps situated 2 mab (m above bottom) were used. They were placed on both sides of the towing area, to account for possible current reverse, and in three rows, approximately 50 m, 150 m and 400 m from the tow zone. Two current meters with nephelometers were deployed 2 mab with sediment traps 5 mab on both sides of the towing zone. During the operation, three sediment traps and one current meter mooring were recovered in order to monitor the progress of the sediment plume dispersion.

Description of model application

Bathymetric data. The digital bathymetric data from the BIE surroundings were obtained from NOAA. The data are available with a resolution of 100 m covering a rectangular area of 14.5 × 11.1 km. The position of the lower left corner of this area (i.e. south) is known exactly, longitude -128.6666° (W) and latitude 12.8833° (N). The depths are given with an accuracy up to a decimeter. The water depths vary between 4692 m and 4929 m (Figure 1).

Computational mesh. Because of the greatest interest in the deposition in the direct vicinity of the tracks and the data availability of only up to a distance of approximately 500 m from them, a mesh for the near field was constructed (Figure 2). Its rectangular shape (3.5 × 4 km) takes into account the fact that the mean current direction during the experiment was NW and the greatest deposition took place in this direction away from the tracks. In the area where the discharge and greatest deposition took place, the mesh resolution is 50 m. The lacking node depths were obtained by interpolating the original data. This area is a rectangle 4 × 1.5 km, with the longer side running approximately parallel to the disturber tracks. The tracks are situated at a distance of 500 m from the south edge of the mesh, leaving a

1000 m broad region NW of the tracks with higher resolution, where the greatest accuracy is needed. NW of this rectangle, two zones of lower resolution between the nodes follow, 100 m and 200 m respectively, each approximately 1000 m broad. The water depths in this area vary between 4887 and 4790 m, $x \in (4350, 9750)$ m, $y \in (3450, 9850)$ m. The basic 2D-mesh consists of 6135 triangular elements and 3138 nodes. The vertical resolution (23 levels) varies between 0.5 m and 10 m up to 50 m above bottom, and then diminishes to 100 m. The upper limit of the computational domain is set by 500 m above bottom. As a result, the 3D mesh has 72174 nodes and 134970 prismatic elements.

Disturber movements and tracks. It is assumed that each tow is performed along the same path defined by the extreme points of the disturber tracks given in Table 2. The distance between these points and the SW and NE mesh edges amounts to 300 m, and from the SE edge about 500 m (Figure 2). The disturber was towed from SW to NE with a ship velocity of about 1 knot, i.e. 0.5 m/s. The track length was about 3300 m. After completing a tow, the disturber was lifted, the ship made a loop, and the procedure repeated. During 19 days 49 tows were completed, an average of 2.6 tows per day. The precise timing of the tows is implemented in the model according to the NOAA cruise report (Trueblood, 1993).

Source strength. The source strength was estimated from the samples of the discharged material collected using a rosette sampler situated at the top of the disturber discharge pipe. The samples yielded an average outlet concentration of 33.3 g/l dry weight. The pump rate is about 125 l/s. The average mass discharge rate can be estimated as 4.17 kg/s dry weight. The total discharged sediment dry mass during 98 h of deployment was estimated to be equal to 1468.5×10^3 kg. The height of the outlet of the discharging pipe (diameter 305 mm), measured from the base of the disturber sleds, varied from tow to tow between 4.33 m and 5.66 m. Shallow water tests have shown that the momentum of jet-like discharge is enough to lift the sediment slurry up to about 10 m above bottom.

In the model, the mass volume source has the same form as in a mesoscale model of DISCOL area (Jankowski et al., 1996):

$$q_c = q_0 \exp\left(-\frac{(x - m_1)^2 + (y - m_2)^2}{2\sigma_1\sigma_2}\right) \exp[-\gamma(z - z_B)] \quad (14)$$

where (m_1, m_2) is the position of the moving source and z_B the coordinate of the bottom. $z \in (z_B, z_M)$, so that the mass discharge reaches zero at a calibrated height z_M above the bottom. Therefore, the distribution of the mass production in the volume is Gaussian in the horizontal and exponential in the vertical direction. It can be characterized by parameters σ_1 , σ_2 and γ . This form of volume source allows taking into account the density effects which cannot be resolved in the given time and space resolutions. However, this distribution dictates the adequate spatial model resolution in the whole area of emission in order to secure a stationary discharge rate. The

overall volume source intensity is controlled by the parameter q_0 ($\text{kg}/\text{m}^3/\text{s}$). The assumed values of σ_1 and σ_2 are 25 m and correspond to the distance between the nodes. γ is assumed to be equal to 0.5 m^{-1} and z_M is equal to 10 m. q_0 is calibrated in order to obtain an approximately stable discharge of 4.2 kg/s independent from the movement or the position of the source. The resulting maximum concentrations on the mesh nodes were in the range of ca. 50 mg/l.

Sediment settling velocity. A mean settling velocity computed from a settling velocity distribution for a concentration of approx. 15 mg/l is given in Table 3 (Lavelle, 1987). It is equal to 1.2×10^{-4} m/s.

Sediment traps. The sediment traps deployed during the NOAA BIE were 1 m long PVC cylinders with an opening of 100 cm^2 . They were deployed in pairs 2 m above bottom (mab). A few traps were situated at 5 mab and combined with current meters and transmissometers; some of them were removed during the experiment for control reasons (Trueblood, 1993). For comparison of the results, only those traps were chosen which were deployed for the whole discharge time and situated 2 mab. The GPS positions of the traps are not in coincidence with the digital bathymetric data, particularly concerning the mooring depth. For this reason, it is assumed that the horizontal coordinates of the traps are exact, but the vertical are changed to 2 m above the bottom coordinate given by the bathymetric data (Table 4).

BIE current analyses. From all available current measurements (Figure 3), the results from the mooring NOAA 21 (position of trap #1, 5 mab) are used to obtain the current scenario. Current characteristics are given in Table 5. The current is characterized by a large stability factor of 0.94 (SF=1 stands for constant current direction):

$$SF = v_{vect}/v_{scal} \quad (15)$$

where v_{scal} and v_{vect} are mean scalar and vector speed:

$$v_{scal} = \frac{1}{n} \sum_{i=1}^n (u_i^2 + v_i^2)^{1/2} \quad (16)$$

$$v_{vect} = (\bar{u}^2 + \bar{v}^2)^{1/2} \quad \bar{u} = \frac{1}{n} \sum_{i=1}^n u_i \quad (17)$$

The current Fourier analysis reveals that the greatest kinetic energy corresponds to the tides and waves in the inertial range. A periodogramme of the currents measured at the NOAA 21 station is shown in Figure 4.

Model forcing. The method of obtaining the model current scenario is the same as in the previous model applications (Jankowski and Zielke, 1995; Jankowski et al.,

1996). The main energy peaks in the spectrum of the current measurements in the BIE area are associated with waves of the radial frequency greater than the inertial one, $\omega > f$. In order to obtain a current scenario for the modeling, a number of frequencies in the sub-inertial range (inertial period $T_f = 53.48$ h) is used (Table 6). Peaks corresponding to these frequencies can be easily recognized in Figure 4. The directions and parameters describing current ellipses for given wave frequencies are obtained by best-fit approximation. The slowly varying components with periods larger than the inertial one are obtained from Fourier approximation by filtering appropriate frequency ranges. A comparison between the approximated currents and measurements for the current meter position is presented in Figure 5.

Other simulation parameters. The non-hydrostatic code version is applied. The horizontal viscosity and sediment diffusivity are assumed to be constant, $1.0 \text{ m}^2/\text{s}$. The parameter controlling the bottom boundary layer thickness and vertical viscosity and diffusivity distribution (i.e. the mixing length scale) is $\delta = 5$ m. The roughness coefficient is calibrated in order to obtain appropriate bottom roughness. The Coriolis parameter is $f = 3.2642015 \times 10^{-5}$ rad/s. Time step is equal to 60 s. The simulation start time is August 14, 0600, the first discharge took place 89 minutes later. The simulation stops after 25 days, about 6.5 days after the last discharge.

Parameter studies. A few parameter studies have been performed, varying the most critical parameters around the values presented above. Only five cases will be mentioned here. In two runs only the settling velocity w_s has been modified to values of 5.0×10^{-4} m/s and 0.2×10^{-4} m/s. In a third one, only the mixing length scale has been enlarged up to $\delta = 20$ m. In the fourth case, only $\gamma = 0.1 \text{ m}^{-1}$, shifting the vertical source strength distribution higher above the bottom. In the fifth case, the horizontal diffusivity and viscosity has been reduced to $0.1 \text{ m}^2/\text{s}$.

Results

Deposition at the bottom. The final sediment deposition at the bottom varies in the computational domain between 0.08 and $1873 \text{ g}/\text{m}^2$. Using the bulk density of freshly deposited sediments of $150\text{--}200 \text{ kg}/\text{m}^3$ the greatest deposition thickness is $9.4\text{--}12.5$ mm, which is confirmed by the post-impact observations. The largest deposition fluxes occur in the deeper situated places along the disturber path (Figure 6). In Figure 7, the lower ranges of deposition are shown in order to estimate the reach of the area where deposition occurs. The distance between the tracks and the SE domain range is sufficient. At the NW edge, the greatest deposition reaches $25 \text{ g}/\text{m}^2$, i.e. 0.03 mm. Due to the non-hydrostatic and stratification effects, the deposition pattern is influenced by bathymetry. Bottom deposition and flux 2 mab (i.e. at the trap level) at the mesh nodes nearest to the positions of these sediment traps, which were deployed during all 49 tows, are shown in Table 4 and in Figure 8.

Mass balances. The total mass of sediment at the bottom after 20 days of simulation is 1345×10^3 kg. This means that over 90% of discharged mass is deposited within the computational domain. The discharged mass in the model is 98% of the estimated 1427 t suspended during the BIE (Table 7). The resuspended mass balance is shown in Figure 9.

Concentration in the water column. Due to the character of the discharge (3 times daily for 90 minutes), no coherent plumes could build up, just disjointed streaks. An example of the plume which resulted during the emission (first tow) is shown in Figure 10.

Parameter studies. Increasing the settling velocity w_s yields much greater discrepancies between the measured and computed trap deposition values, while the pattern 2 mab and on the bottom remain very similar. Decreasing w_s yields a bottom deposition very similar to the measurements, while the flux 2 mab, especially for the downstream traps, is much larger than observed. The maximum deposition values are 2700 g/m^2 and 750 g/m^2 . Enlarging the thickness of the bottom boundary layer brings a similar distribution to the one shown in Figure 8, but with lower deposition (max. value 560 g/m^2). The deposition pattern is much less sensitive to the bathymetry. Shifting the mass source distribution higher (case 4) delivers similar deposition patterns again, with max. value of 655 g/m^2 , while the deposition in the upstream traps is enhanced. Lowering the horizontal diffusivity (case 5) increases the deposition near the tracks, but due to the larger densities, the deposition pattern is locally widespread with maximum deposition of 1580 g/m^2 .

Conclusions

Although the model reproduces the overall bottom deposition pattern and the coverage thickness is comparable to the observed one, the comparison with trap measurements is not very satisfactory. The flux 2 mab and the bottom deposition is larger compared to the sediment trap data. Shifting the vertical position of the mass discharge intensity center does not change this situation, nor does decreasing the settling velocity or enhancing the stratification. Excluding the bottom boundary layer thickness from the discussion (not precisely known), the most probable reason for differences can be the imperfect reproduction of the source movements. In the model, a firm trajectory of the disturber was assumed. In reality, the trajectories varied in lengths and directions during the tows so that a directly disturbed track of ca. 150 m width was produced. Another source of errors may be the mass source parameterization according to (14), as well as difficulties in measuring fluxes using sediment traps (Gust et al., 1994). There are some uncertainties in the trap positions as well. The bottom sampling in the BIE area provides evidence that there is a large discrepancy between the deposition at the bottom and sediment trap contents (Trueblood, 1993), which was interpreted as density current influence. As a

confirmation, the greatest discrepancies occur in the model for traps #12, #14, and #15. They are situated at the SE side of the towing zone, i.e. against the prevailing current. In addition to the aspects mentioned above, for future applications more information is needed about the vertical structure of the near field plume and parameters characterizing the bottom boundary layer.

Modeling in the DISCOL Experimental Area

Sediment transport

It was hoped that new current measurements performed in the DISCOL area (Klein, 1996) and sediment properties investigations (Becker et al., 2001; Grupe et al., 2001; Oebius et al., 2001) would yield substantial support data for mesoscale modeling. During these current measurements (short-term, the longest deployment 52 days), a period of extremely low velocities in the range or lower than the meter threshold velocity (1-1.5 cm/s) appeared, resulting in rotor stalls in the range of 46-89%. The currents were very weak and very unstable in their direction. Therefore, no additional information to that of the previous measurements (Klein, 1993) concerning the bottom boundary layer characteristics could be obtained. Due to equipment failure, the planned *in situ* investigations regarding the sediment properties had to be substituted by laboratory experiments.

Most important for the model data support are the sediment particle spectra, allowing an estimate of the suspended sediment settling velocity. The previously available spectrum (Table 1, (Klein, 1993)) has a mean settling velocity $w_{sm} \approx 2.2 \cdot 10^{-4}$ m/s. The new, more exact spectra, obtained using laser technique (Grupe et al., 2001; Oebius et al., 2001) yield slightly smaller values of w_{sm} in the range of $1.2 - 1.6 \cdot 10^{-4}$ m/s. These, however, are still higher than the settling velocity value assumed to be representative for conservative estimates (Jankowski et al., 1996; Jankowski and Zielke, 1995). Other estimates yield mean settling velocities one magnitude larger than previously estimated (Nakata et al., 1997), see (Oebius et al., 2001). No quantitative data are available for a theoretically developed flocculation model for suspended deep-sea sediment (Jankowski et al., 1996).

For these reasons, there is no evidence available that would change the conclusions formulated on the basis of parameter studies done in the DISCOL area and previously documented by the authors (Jankowski and Zielke, 1995; Jankowski et al., 1996). The conclusions of these studies are summarized in (Thiel and Forschungsverbund Tiefsee-Umweltschutz, 2001). The following section provides only a short description relevant to heavy metal transport (next section).

The mesoscale regional model was developed for the ca. 500 km² large surround-

ings of the DISCOL Experimental Area (DEA) centered about 7° 04' S, 88° 28' W in the Peru Basin. The size of this region allows the simulation of a plume spreading during 1–2 weeks, depending on the current magnitude. Two typical current scenarios were implemented. The near bottom suspended sediment emissions lead to a substantial impact mainly on a local scale. The use of available support data from the DISCOL Experimental Area yields plume residence times in the order of 1.5–6 days. The model is adjusted to the mining operation expected during pilot mining or benthic impact experiments with the hope of obtaining better validation conditions. The discharge is low, 10 kg/s, in a relatively small area (path length about 1500 m) and limited in time (1–6 days). Extensive parameter studies were carried out. Different constant mean settling velocities (with the most realistic value assumed to be 10^{-4} m/s) and a composite spectrum of settling velocities for non-cohesive sediment classes (*a – e*) according to Table 1 were applied (Figure 11). For a discharge of 100 kg/s (Oebius et al., 2001), which is probably twice too large for this device velocity, only slight differences in the settling rate of the suspended mass are observed. A simple extrapolation of the concentrations and the bottom blanketing is possible with an acceptable error in the range of up to 100 kg/s. The shape of the curves confirms that the ratio of the suspended to the discharged mass diminishes over time.

The results for a discharge of 10 kg/s lasting for 1 day and with settling velocities in the range of $10^{-5} - 10^{-4}$ m/s indicate concentration in the plume up to 50 times above ambient (taken as $10 \mu\text{g/l}$). For a continuous discharge, this level of concentrations is reached in the plume after 6 days about 15 km away from the source. For the one-day-discharge, only a few percent of the discharged mass is present in the water column as the finest particles, compared to 10% for continuous source. The sea bed will be covered with $> 100 \text{ g/m}^2$ of sediment in a radius of approximately 1–2 km from the collector tracks. With continuous discharge this area remains similar, but the deposition near the tracks can reach even 5 kg/m^2 or about 30 mm. These values can be recomputed for larger discharges in a linear way without larger errors.

Mobilization, sorption and transport of heavy metals

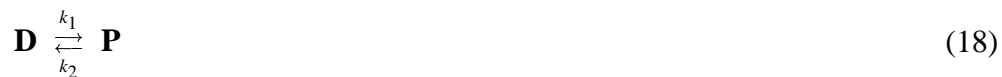
The interstitial water, released to the water column together with the stirred bottom sediments, is thought to be a source of substances that may be harmful to marine organisms. The greatest concern is about dissolved toxic heavy metals. After release, they will passively follow the water movements while interacting with the surrounding particles of different sorption properties. The disturbance may change the physico-chemical properties of the environment influencing the metal distribution between dissolved and solid phases and, consequently, their availability and toxicity to marine organisms (Koschinsky et al., 1997; 2001a). The metals bound to the particles may eventually settle to the bottom (if not released from them be-

fore). As another potential source of mobilized heavy metals, the abraded nodule fines (by changed physico-chemical environment of the surrounding water) should also be mentioned.

Heavy metals will be discharged along with the sediment particles. Special attention is paid to *Mn*, *Co*, *Zn*, *Cd*, *Fe*, *As*, *Cs* and *Hg* (Koschinsky et al., 1997). The interaction between the various mobilized substances is considered by additional source terms in the transport Equation (7), whereby the dissolved substances move passively with the current ($w_s = 0$), and the bound ones settle with the sediment. A proper description of the sorption-desorption interactions is important for environmental impact assessment because they control the heavy metal bio-availability. In order to deal with this problem, an additional step of the numerical algorithm has been developed in the framework of operator splitting which solves a set of coupled non-linear differential equations with the Runge-Kutta method of the fourth order. This step allows modeling complex interactions among a number of substances which may take place in other timescales than the hydrodynamic processes and, therefore, are treated with different time resolution. This is a well-validated approach for water quality applications (Orlob, 1983; Onishi, 1994).

However, due to the fact that the exact description of the sorption kinetics in the deep sea is the matter of further research and known only approximately, first-order models for the heavy metal cycling in aquatic systems are applied in practice (Nyffeler et al., 1984; Cowen et al., 1990; Lavelle et al., 1992). An equilibrium approach to sorption dynamics can hold only when the time scales of interest are much larger than the time scales of adsorption and desorption processes (Imboden, 1978). In this case, the dynamic balance of two opposite processes can be treated as a steady state partitioning between dissolved and bounded (particulate) forms. Otherwise, a kinetic approach must be applied. This is especially the case when the metals are mobilized by man-made disturbances that are variable in time.

In the developed model, a kinetic (non-equilibrium) approach is implemented. Its properties are best understood assuming a constant total concentration of all phases as well as of the suspended sediment. This is satisfied in laboratory experiments – a closed system compared to an open one. The sorption and desorption process in which the dissolved **D** and the particle bound **P** metal is involved can be visualized as:



With c_d the dissolved metal concentration, c_p the adsorbed metal concentration on sediment particles (particulate phase) measured in $[\text{kg}/\text{m}^3]$, and $c_0 = c_p + c_d$ the total concentration, a one-stage sorption/desorption process can be described as:

$$\begin{aligned}\frac{dc_d}{dt} &= -k_1c_d + k_2c_p \\ \frac{dc_p}{dt} &= +k_1c_d - k_2c_p\end{aligned}\tag{19}$$

where k_1 is the sorption rate and k_2 the resorption rate (in $[\text{s}^{-1}]$ or $[\text{d}^{-1}]$). In general, these rates are functions of particle properties (e.g., their concentration, surface type), sorption mechanisms, dissolved species, and pH, and are very specific for a given aquatic system. For further considerations, it is assumed that k_1 and k_2 are not functions of c_d or c_p . The solution of the Equations (19) are the following exponential functions of time:

$$\begin{aligned}\frac{c_d}{c_0} &= \frac{k_2}{k_1 + k_2} + \frac{k_1}{k_1 + k_2} \exp[-(k_1 + k_2)t] \\ \frac{c_p}{c_0} &= \frac{k_1}{k_1 + k_2} - \frac{k_1}{k_1 + k_2} \exp[-(k_1 + k_2)t]\end{aligned}\tag{20}$$

The distribution coefficient $k_D(t) = c_p(t)/c_d(t)$ is given as:

$$k_D(t) = \frac{c_p(t)}{c_d(t)} = \frac{k_1 - k_1 \exp[-(k_1 + k_2)t]}{k_2 + k_1 \exp[-(k_1 + k_2)t]}\tag{21}$$

for $t \rightarrow \infty$ the distribution coefficient is equal:

$$k_D = \frac{k_1}{k_2} = \frac{c_p}{c_d}\tag{22}$$

and can be immediately obtained when steady state $dc_p/dt = dc_d/dt = 0$ is assumed.

While the resorption rates for the metals of interest found in literature do not vary much (magnitude order about 0.1–2.0 d^{-1}), the adsorption rates vary strongly and depend on the suspended sediment particle concentration c (Nyffeler et al., 1984). This concentration can be taken into consideration assuming that the sorption rate $k_1 = k_1(c)$, while $k_2 = \text{const}$, which is acceptable as the simplest model (Honeyman et al., 1988). Furthermore, it is usually assumed that the distribution constant k_D is a linear function of the sediment concentration c :

$$k_D = \frac{k_1}{k_2} = Kc\tag{23}$$

where K [m^3/kg] is a distribution constant normalized by the sediment concentration. Linearity can be assumed for small variations of c , whereas for larger varia-

tions, a model with exponential dependency of k_D on c would be more appropriate (Honeyman et al., 1988). For a linear dependency, the sorption coefficient can be expressed as:

$$k_1 = k_2 K c \quad (24)$$

and the dependence of the sorbed concentration on the sediment concentration, when the equilibrium is reached, is described by the following isotherms:

$$\begin{aligned} \frac{c_d}{c_0} &= \frac{1}{1 + Kc} \\ \frac{c_p}{c_0} &= \frac{Kc}{1 + Kc} \end{aligned} \quad (25)$$

The values of k_1/c for the metals of interest vary several orders of magnitude between $10^{-3} - 10^2 \text{ m}^3\text{kg}^{-1}\text{d}^{-1}$ (Nyffeler et al., 1984). Consequently, when $k_2 = \text{const}$, values of K vary strongly according to (24). The expressions (20) and (25) can be applied in order to obtain the sorption and resorption rates for various sediment concentrations from the laboratory experiments (Koschinsky et al., 1997; 2001a). Examples of the sorption curves for various sediment concentrations and realistic rate values are given in Figure 12.

Nyffeler et al. (1984) suggest further that the metals can be divided into two groups of distinct sorption behavior. For the first group, *Na*, *Zn*, *Se*, *Sr*, *Cd*, *Sn*, *Sb*, *Ba*, *Hg*, *Th*, and *Pa*, the one-step sorption model as described before, is appropriate. For these elements, the sorption processes can be described as an overall reversible reaction. For the second group with *Be*, *Mn*, *Fe* and *Co*, a two-stage process is observed. In this case, after sorption at particle surface, a further stage with a long-term sorption appears (explainable as a lattice transport (Nyffeler et al., 1984) or isotopic exchange (Koschinsky et al., 2001b):



where k_3 has an order of magnitude of $0.01-0.05 \text{ d}^{-1}$ and $k_4 \approx 0$ in the time scales of a mesoscale model. Therefore, this second, much slower reaction can be treated as irreversible. When c_l describes the irreversibly sorbed metal concentration, this two-stage process can be described as:

$$\frac{dc_d}{dt} = -k_1 c_d + k_2 c_p$$

$$\begin{aligned}\frac{dc_p}{dt} &= +k_1c_d - (k_2 + k_3)c_p \\ \frac{dc_l}{dt} &= +k_3c_p\end{aligned}\tag{27}$$

As an example, the sorption curves for both metal types and for constant conditions are shown in Figure 13.

The rates describing the kinetics assume values obtained for the bottom surface sediments from MANOP Site H in concentration of 0.1 g/l published by Nyffeler (Nyffeler et al., 1984) and are presented in Table 8.

For a rigorous description of the system, all reactions of the dissolved element with the solid phase must be known and the reaction rate constants for various suspended sediment concentrations quantified. Unfortunately, *in situ* measurements are complicated, especially in deep-sea conditions (Koschinsky et al., 1997). Also, an application of rates from a different aquatic system to the deep-sea environment is not appropriate (Nyffeler et al., 1984). The deep-sea rates are only roughly known from laboratory experiments under conditions occurring in nature (e.g. temperature, salinity, pH, but not pressure) and using original particles. However, the assumption of an open system is not valid in this case and no realistic biological influence can be observed.

In the case of deep-sea mining discharges, the total concentration c_0 of the metal in the water column within a given domain changes in time and space due to the man-made discharge, advective and diffusive transport and settling of the sediment particles containing sorbed metals. The assumption of a closed system (as in a laboratory) is not valid. It is assumed that the metals are discharged in a constant ratio of the dissolved to the particulate phases $k_{dis} = c_p/c_d$ with rates of q_{c_d} and q_{c_p} . These phases are computed from the dissolved metal concentrations in the interstitial water. The term q_{c_d} is connected strictly with the discharge rate for the sediment q_c . There are two mechanisms of the particle-bound metal removal from the water column. First, the particles settle with the settling velocity of the sediment w_s , second, they are scavenged by marine snow with a rate represented by a source term q_s . Very little is known about the diffusion from the tracks of the mining devices and the diffusion from freshly deposited particles. The small diffusive flux of the dissolved metal can be made proportional to the settling flux of contaminated particles if the appropriate rates are known (Lavelle et al., 1992). For environmental impact assessment, metals in the particulate phase, which reach the bottom sediments, are treated as removed from the system. The sediment erosion (including contaminated particles) and the diffusion of the dissolved metals from the bottom sediments to the water column are assumed to be negligible.

The processes discussed above are schematically presented in Figure 14. The mathematical description of the concentration development of metal phases results in

three transport equations. These have to be solved simultaneously with the sediment transport Equation (7):

$$\frac{\partial c_d}{\partial t} + u \frac{\partial c_d}{\partial x} + v \frac{\partial c_d}{\partial y} + w \frac{\partial c_d}{\partial z} = \quad (28)$$

$$\frac{\partial}{\partial x} \left(v_{xc} \frac{\partial c_d}{\partial x} \right) + \frac{\partial}{\partial y} \left(v_{yc} \frac{\partial c_d}{\partial y} \right) + \frac{\partial}{\partial z} \left(v_{zc} \frac{\partial c_d}{\partial z} \right) - k_1 c_d + k_2 c_p + q_{c_d}$$

$$\frac{\partial c_p}{\partial t} + u \frac{\partial c_p}{\partial x} + v \frac{\partial c_p}{\partial y} + w \frac{\partial c_p}{\partial z} + \frac{\partial (w_s c_p)}{\partial z} = \quad (29)$$

$$\frac{\partial}{\partial x} \left(v_{xc} \frac{\partial c_p}{\partial x} \right) + \frac{\partial}{\partial y} \left(v_{yc} \frac{\partial c_p}{\partial y} \right) + \frac{\partial}{\partial z} \left(v_{zc} \frac{\partial c_p}{\partial z} \right) + k_1 c_d - (k_2 + k_3) c_p + q_{c_p} + q_s$$

$$\frac{\partial c_l}{\partial t} + u \frac{\partial c_l}{\partial x} + v \frac{\partial c_l}{\partial y} + w \frac{\partial c_l}{\partial z} + \frac{\partial (w_s c_l)}{\partial z} = \quad (30)$$

$$\frac{\partial}{\partial x} \left(v_{xc} \frac{\partial c_l}{\partial x} \right) + \frac{\partial}{\partial y} \left(v_{yc} \frac{\partial c_l}{\partial y} \right) + \frac{\partial}{\partial z} \left(v_{zc} \frac{\partial c_l}{\partial z} \right) + k_3 c_p + q_s$$

In the case of settling particles, the boundary conditions for sediment are assumed. For dissolved species, a no-flux boundary condition at the bottom and model surface is applied. In all cases the substances may leave the lateral computational domain boundaries freely.

Results and conclusions for the heavy metal transport

If one fits the experimental data for fine suspended sediment, $d < 63 \mu\text{m}$; $c = 0.1, 1, 10, \text{ and } 30 \text{ g/l}$ (Koschinsky et al., 1997), to Equation (20), one obtains similar adsorption coefficients as given by Nyffeler et al. (1984), but different values for resorption and K .

The results suggest that for Mn , the value of k_2 is at least one order of magnitude greater ($0.2 - 0.5 \text{ d}^{-1}$). K varies strongly and proportionally to c , from $50 - 500 \text{ m}^3\text{kg}^{-1}$, which suggests an exponential dependency of k_1 on c for larger sediment concentrations. For Co , $k_2 \approx 0.8 - 1.2 \text{ d}^{-1}$ and $K \approx 50 - 500 \text{ m}^3\text{kg}^{-1}$. For low-reactive Cs , the values are in good agreement with MANOP data, $k_2 = 1.0 - 2.0 \text{ d}^{-1}$, $K = 0.1 - 1.0 \text{ m}^3\text{kg}^{-1}$.

The laboratory experiments were performed for a time period of about 7 days, so that no information is available for the long-term two-stage sorption processes. For modeling, literature values are assumed (Nyffeler et al., 1984). Due to the fact that the suspended sediment concentrations are lower than applied in the laboratory experiments, the values obtained for fitting $c = 0.1 \text{ g/l}$ are assumed.

The concentrations in the interstitial water c_b , from which the discharge rate is computed, are $27.47 \mu\text{g/l}$ (500 nmol/l) for *Mn* and $0.95 \mu\text{g/l}$ (7 nmol/l) for *Cs* (Koschinsky et al., 1997). k_1 varies according to (24). $47 \mu\text{g Mn}$ and $1.65 \mu\text{g Cs}$ along with 1 kg sediment are discharged assuming the bottom sediment porosity of 0.82 . k_{dis} is taken to be equal to $1/9$ for both cases.

The results are shown in Figures 15 and 16 in form of mass balances for a discharge period of 1 day and a continuous discharge of 7 days. A current scenario with larger speeds is assumed (Jankowski et al., 1996), and other parameters are $w_s = 10^{-4} \text{ m/s}$, $\delta = 10 \text{ m}$, $v_h = 1.0 \text{ m}^2/\text{s}$. For low reactive *Cs* (note the logarithmic mass scale), a constant distribution value k_D between the dissolved and particulate phase is achieved only by continuous discharge. This guarantees a relatively constant spatial distribution of sediment concentration. By an interrupted discharge, the sediment concentration diminishes in time, and the particle-bound *Cs* settles to the bottom so that the dissolved metal mass remains constant.

Similar interpretation can be given for *Mn*, but with much larger sorption dynamics. In the case of the described model, the value of the resorption constant k_2 plays a significant role. Away from the source, the difference between the settling of particle-bound metals and the movement of dissolved metals is very important. It leads to resorption of the metals from the particles in the bottom-near zone and weakening of sorption of dissolved species higher above. The value of the resorption coefficient plays the key role. This can be best illustrated by an example, whereby mass balances for two hypothetical metals discharged for a day duration with k_2 differing about one order of magnitude, but with identical k_1 values (K changes accordingly), are compared (Figure 17). For simplicity, $k_3 = 0$. When the discharge stops, the mass of particle-bound metal is much larger in case of lower resorption coefficients.

In conclusion, the model indicates that for continuous discharges, the expected equilibrium distribution between the particle-bound phase and the solute one is reached. However, there are situations when particle settling and current shear in the bottom boundary layer may lead to a separation of the phases. The model presented indicates that only in this case the dissolved species may remain longer in the water column or it may come to resorption. However, the values of the coefficients must be known more exactly in order to formulate reliable environmental impact assessments. There is evidence that it may also be necessary to include further geochemical processes in the model (Koschinsky et al., 1997).

Summary

The developed numerical model allows the simulation of transport within the deep-sea bottom boundary layer. The hydrodynamic module takes into consideration

the typical phenomena occurring there, including variable bathymetry influence, bottom shear, and stratification effects. All modeling parameters can be obtained from measurements *in situ* or from fluid properties. A reliable method for obtaining the current variability in time has been developed based on Fourier analysis of the current measurements. It produces current scenarios representative for the bottom-near zone of the ocean. This method is independent from the particular mining area. In addition to the local bathymetry it requires some prior knowledge of the area's hydrography in form of current measurements within the bottom boundary layer and/or above it. The approach is appropriate for simulation times of up to a few weeks in areas of an extent up to 1000 km².

The transport module allows simulation of suspended sediment transport including its deposition to the bottom. The stratification effects are taken into consideration in the mixing length turbulence model. The concentration model requires a careful idealization of the source of the suspended sediment. The area in which the discharge takes place must be resolved with appropriate mesh spacing so that both discharge rate and concentration are well reproduced. For the mesoscale model, a horizontal resolution of 50–100 m and a vertical in the range 0.5–1 m are required. The applied mesh is unstructured and the resolution may be much less at a greater distance from the source. The only requirement is to reproduce bathymetry properly.

The model allows various treatments of the sediment settling velocity, with or without taking the cohesive sediment properties into account. In theory, all common approaches are possible in the framework of the concentration model. In practice, assumptions of constant mean settling velocity or taking a few settling velocity classes have proved to be appropriate. A theoretical sediment flocculation model, based on empirical constants that can experimentally be obtained, has been developed (Jankowski et al., 1996).

The simulation of further effluents along with sediments is realized by solving a transport equation for each phase. The interaction between these phases is taken into consideration by the source terms in equations. The model has been applied for transport of heavy metals discharged from the interstitial water. Both kinetic and equilibrium approaches are possible. The kinetic approach should be chosen not only when the sorption time scales are large, but also when the concentration variability due to various discharge intensities is considerable.

The results for the sediment transport based on the BIE data show that even without appropriate information (bottom boundary layer characteristics, suspended sediment parameters and source characterization) the model is capable of reproducing the bottom deposition fairly well. Discrepancies exist with regard to the sediment trap measurements, whose data, however, may not be sufficiently accurate for model validation. Unfortunately, the predictions for larger areas must still be treated with caution due to the insufficient quality of support data (Jankowski and

Zielke, 1997). Model-oriented data sampling during field experiments may improve the forecast reliability.

The computed results for the transport of the heavy metals interacting with the sediment particles are obtained with a first-order model, with sorption rates that are known only approximately. The feasibility of the model to deal with this task is presented. However, a substantial input of support data, also influencing model assumptions, is still needed. The results indicate that the values of interaction rates, especially the resorption rate, are important for the bio-availability of the heavy metals at a distance from the source.

Acknowledgements

The research work was sponsored by the German *Bundesministerium für Bildung und Forschung (BMBF)* within the interdisciplinary research group TUSCH under grant 03 G 0106 C *Mesoskalige Stofftransporte im Pazifik als Folge technischer Eingriffe in die Tiefsee (TRANSMOD I)*. The authors are solely responsible for the contents of this paper. The computer code TELEMAC3D was developed by Laboratoire National d'Hydraulique in Chatou by Paris (Electricité de France). The authors thank Dr. E. Ozturgut and Dr. W. Lavelle (PMEL NOAA Seattle, USA) for making the NOAA BIE data available and fruitful discussions.

References

- Becker, H.-J., Grupe, B., Oebius, H., Liu, F., 2001. The behavior of deep sea sediments under the impact of nodule mining processes. *Deep-Sea Research II*.
- Bischoff, J., Heath, G., Leinen, M., 1979. Geochemistry of deep-sea sediments from the Pacific manganese nodule province: DOMES sites A, B, and C. In *Marine Geology and Oceanography of the Pacific Manganese Nodule Province*, J. Bischoff and D. Piper, Eds., Plenum Press, pp. 397–436.
- Brockett, T., Richards, C., 1994. Deepsea mining simulator for environmental impact studies. *Sea Technology*, 1994(8), 77–82.
- Cowen, J., Massoth, G., Feely, R., 1990. Scavenging rates of dissolved manganese in a hydrothermal vent plume. *Deep-Sea Research*, 37, 1619–1637.
- Fukushima, T., 1995. Overview Japan Deep-Sea Impact Experiment = JET. In *Proceedings of the First (1995) ISOPE Ocean Mining Symposium*, Tsukuba, Japan, ISOPE, pp. 47–53.
- Galland, J.-C., Goutal, N., Hervouet, J.-M., 1991. TELEMAC: A new numerical model for solving shallow water equations. *Adv. Water Resources*, 14(3), 138–148.

- Grupe, B., Becker, H.-J., Oebius, H., 2001. Geotechnical and sedimentological investigations of deep-sea sediments from a manganese nodule field of the Peru Basin. *Deep-Sea Research II*.
- Gust, G., Michaels, A., Johnson, R., Deuser, W., Bowles, W., 1994. Mooring line motions and sediment trap hydromechanics: in situ intercomparison of three common deployment designs. *Deep-Sea Research*, 41(5/6), 831–857.
- Hill, P., Nowell, A., 1995. Comparison of two models of aggregation in continental-shelf bottom boundary layers. *Journal of Geophysical Research*, 100(C11), 22,749–22,763.
- Honeyman, B., Balistieri, L., Murray, J., 1988. Oceanic trace metal scavenging: the importance of particle concentration. *Deep-Sea Research*, 35, 227–246.
- Imboden, D., Lerman, A., 1978. Chemical models of lakes. In *Lakes – chemistry, geology, physics*, D. Imboden, Ed. Springer Verlag, Heidelberg, Berlin, New York, pp. 341–356.
- Jankowski, J., 1999. A non-hydrostatic model for free surface flows. PhD thesis, Universität Hannover. Bericht Nr. 56/1999, Institut für Strömungsmechanik und ERiB.
- Jankowski, J., Malcherek, A., Zielke, W., 1994. Numerical modeling of sediment transport processes caused by deep sea mining discharges. In *Proceedings of the OCEANS 94 Conference, Brest*, vol. III, IEEE/SEE, pp. 269–276.
- Jankowski, J., Malcherek, A., Zielke, W., 1996. Numerical modelling of suspended sediment due to deep-sea mining. *Journal of Geophysical Research*, 101(C2), 3545–3560.
- Jankowski, J., Zielke, W., 1995. Mesoskalige Stofftransporte im Pazifik als Folge des Tiefseebergbaus. Final report, Institut für Strömungsmechanik und ERiB, Universität Hannover. 86 pp.
- Jankowski, J., Zielke, W., 1997. Data support for modelling of deep-sea mining impacts. In *Proceedings of the Seventh (1997) International Offshore and Polar Engineering Conference, Honolulu, USA*, vol. I, International Society of Offshore and Polar Engineers, pp. 451–460.
- Klein, H., 1993. Near-bottom currents in the deep Peru Basin, DISCOL Experimental Area. *Deutsche Hydrographische Zeitschrift*, 45, 31–42.
- Klein, H., 1996. Near-bottom currents and bottom boundary layer variability over manganese nodule fields in the Peru Basin, SE Pacific. *Deutsche Hydrographische Zeitschrift*, 48, 147–160.
- Koschinsky, A., Gerber, H., Szemeitat, A., 1997. Experiments on the influence of the technical activities in the deep-sea on heavy metal cycles. In *Proceedings of the Seventh (1997) International Offshore and Polar Engineering Conference, Honolulu, USA*, vol. I, International Society of Offshore and Polar Engineers, pp. 445–450.
- Koschinsky, A., Fritsche, U., Winkler, A., 2001a. Sequential leaching of Peru Basin surface sediment for the assessment of aged and fresh heavy metal associations and mobility. *Deep-Sea Research II*.
- Koschinsky, A., Winkler, A., Fritsche, U., 2001b. Importance of different types of marine particles for the scavenging of heavy metals in the deep-sea. *Applied*

- Geochemistry, submitted..
- Krone, R., 1962. Flume studies of the transport of sediment in estuarial shoaling processes. Final report, Hydraulic Engineering Laboratory, University of California, Berkeley.
- Lavelle, J., 1987. Effects of boundary layer structure and macro-particle scavenging on the benthic deposition of fine sediment resuspended during nodule mining. Final Report to NOAA Office of Ocean and Coastal Resource Management, NOAA Pacific Marine Environmental Laboratory, Seattle. 39 pp.
- Lavelle, J., Cowen, J., Massoth, G., 1992. A model for the deposition of hydrothermal manganese near ridge crests. *Journal of Geophysical Research*, 97(C5), 7413–7424.
- Lavelle, J., Ozturgut, E., Baker, E., Swift, S., 1982. Discharge and surface plume measurements during manganese nodule mining tests in the North Equatorial Pacific. *Marine Environmental Research*, 7, 51–70.
- Lavelle, J., Ozturgut, E., Swift, S., Ericson, B., 1981. Dispersal and resedimentation of the benthic plume from deep-sea mining operations: a model with calibration. *Marine Mining*, 3(1/2), 59–93.
- McCave, I., 1984. Size-spectra and aggregation of suspended particles in the deep ocean. *Deep-Sea Research*, 31, 329–352.
- McCave, I., Gross, T., 1991. In-situ measurements of particle settling velocity in the deep sea. *Marine Geology*, 99(3/4), 403–412.
- McLean, S. R., 1985. Theoretical modelling of deep ocean sediment transport. *Marine Geology*, 66, 243–265.
- Mofjeld, H., Lavelle, W., 1984. Setting the length scale in a second-order closure model of the unstratified bottom boundary layer. *Journal of Physical Oceanography*, 14, 833–839.
- Nakata, K., Kubota, M., Aoki, S., Taguchi, K., 1997. Dispersion of resuspended sediment by ocean mining activity. Modelling study. In *Proceedings of the Symposium on Environmental Studies for Deep-Sea Mining*, Tokyo, Japan, November 20-21, Metal Mining Agency of Japan (MMAJ), pp. 169–186.
- Nyffeler, U., Li, Y.-H., Santschi, P., 1984. A kinetic approach to describe trace-element distribution between particles and solution in natural aquatic systems. *Geochimica et Cosmochimica Acta*, 48, 1513–1522.
- Oebius, H.U. Becker, H.-J., Rolinski, S., Jankowski, J., 2001. Parametrization and evaluation of marine environmental impacts produced by deep-sea manganese nodules mining. *Deep-Sea Research Part II*.
- Onishi, Y., 1994. Contaminant transport modelling in surface waters. In *Proceedings of the NATO Advanced Study Institute on Computer Modeling of Free-Surface and Pressurized Flows*, M. Chaudhry and L. Mays, Eds., no. 274 in NATO ASI series : Series E, Applied sciences, Kluwer Acad. Publ., pp. 313–341.
- Orlob, G., Ed., 1983. *Mathematical modeling of water quality: Streams, lakes and reservoirs*. No. 12 in *Int. Series on Applied Systems Analysis*. Wiley, Chichester, New York. 509 pp.
- Ozturgut, E., Lavelle, J., 1986. Settling analysis of fine sediments in salt water at

- concentrations low enough to preclude flocculation. *Marine Geology*, 69, 353–362.
- Ozturgut, E., Lavelle, J., Erickson, B., 1981. Estimated discharge characteristics of a commercial nodule mining operation. *Marine Mining*, 3(1/2), 1–13.
- Ozturgut, E., Trueblood, D., Lawless, J., 1997. An overview of the United States' Benthic Impact Experiment. In *Proceedings of the Symposium on Environmental Studies for Deep-Sea Mining*, Tokyo, Japan, November 20-21, Metal Mining Agency of Japan (MMAJ), pp. 23–31.
- Rolinski, S., Segschneider, J., Sündermann, J., 2001. Long-term propagation of tailings from deep-sea mining under variable conditions - Numerical simulations. *Deep-Sea Research Part II*.
- Schriever, G., 1995. DISCOL- disturbance and recolonization experiment of a manganese nodule area of the southeastern Pacific. In *Proceedings of the First (1995) ISOPE Ocean Mining Symposium*, Tsukuba, Japan, ISOPE, pp. 163–166.
- Schriever, G., Koschinsky, A., Bluhm, H., 1996. Cruise Report ATESEPP (Impact of potential technical interventions on the deep-sea ecosystem of the southeast Pacific off Peru. Report Nr. 11, Reihe E: Hydrobiologie und Fischereiwissenschaft, Zentrum für Meeres- und Klimaforschung der Universität Hamburg. 195 pp.
- Segschneider, J., Sündermann, J., 1997. Large scale transport of particle reactive tracers – numerical simulations. In *Proceedings of the Seventh (1997) International Offshore and Polar Engineering Conference*, Honolulu, USA, vol. I, International Society of Offshore and Polar Engineers, pp. 461–467.
- Taguchi, K., Nakata, K., Aoki, S., Kubota, M., 1995. Environmental study on the deep-sea mining of manganese nodules in the Northeastern Tropical Pacific. In *Proceedings of the First (1995) ISOPE Ocean Mining Symposium*, Tsukuba, Japan, ISOPE, pp. 167–174.
- Thiel, H., and Forschungsverbund Tiefsee-Umweltschutz, 2001. Evaluation of the environmental consequences of polymetallic nodule mining based on the results of the TUSCH Research Association. *Deep-Sea Research Part II*.
- Trueblood, D., 1993. US Cruise report for BIE II. NOAA Technical Memorandum NOS OCRM 4, NOAA, National Ocean Service.
- Zielke, W., Jankowski, J., Sündermann, J., Segschneider, J., 1995. Numerical modeling of sediment transport caused by deep sea mining. In *Proceedings of the First (1995) ISOPE Ocean Mining Symposium*, Tsukuba, Japan, ISOPE, pp. 157–161.

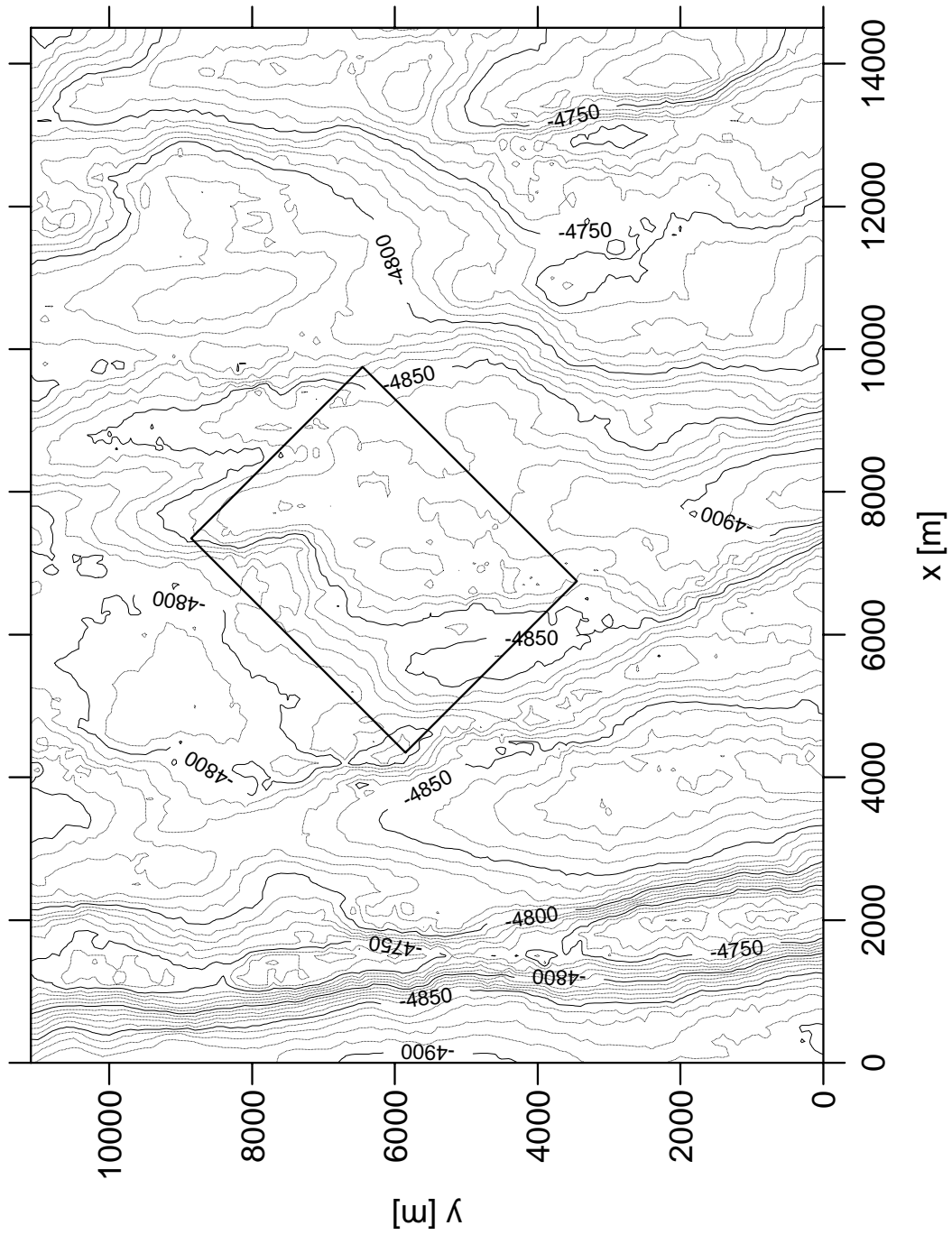


Fig. 1. The bathymetry of the BIE surrounding area. The ranges of computational domain are shown. The coordinate system origin is 128.66667° W, 12.8833333° N.

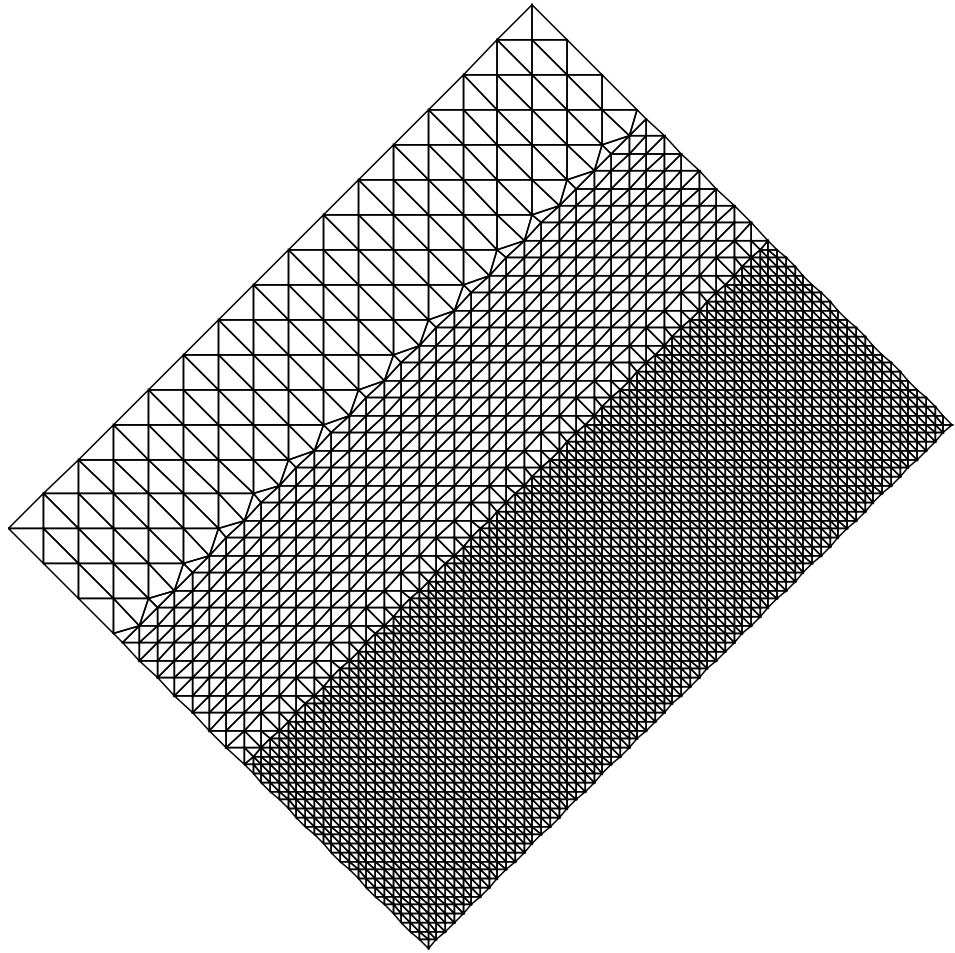


Fig. 2. BIE mesh. Discretization varies between 50 and 200 m.

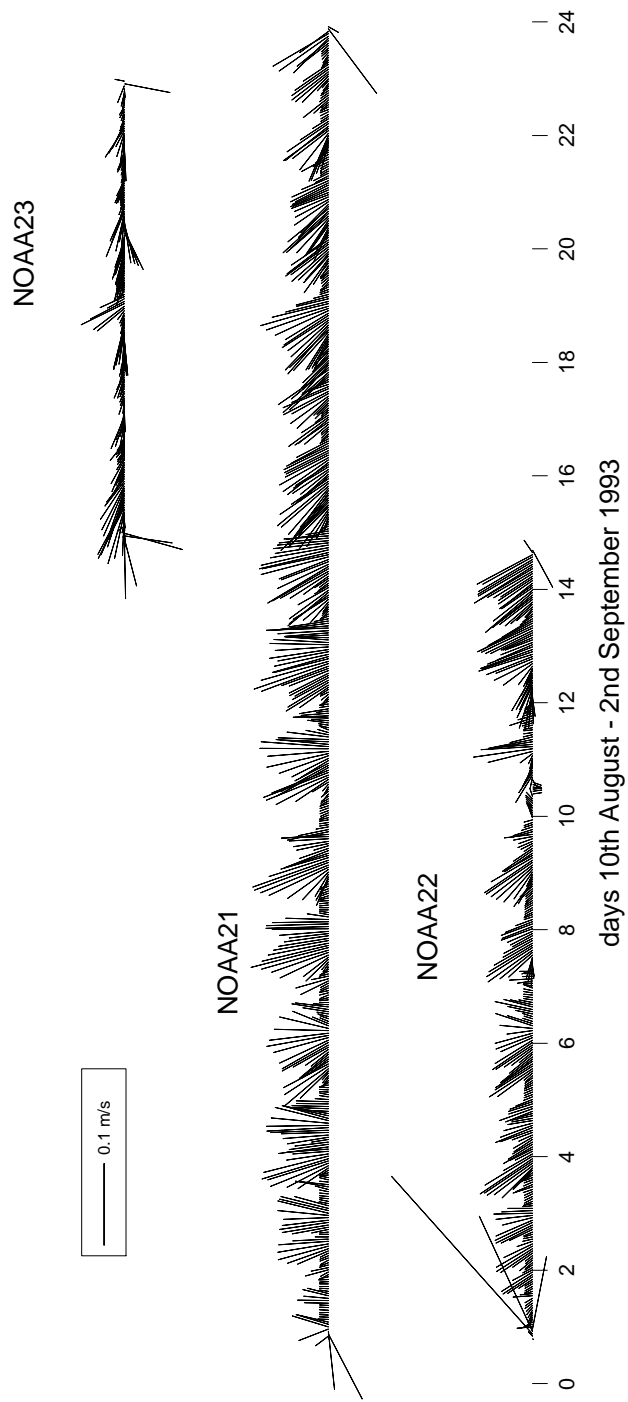
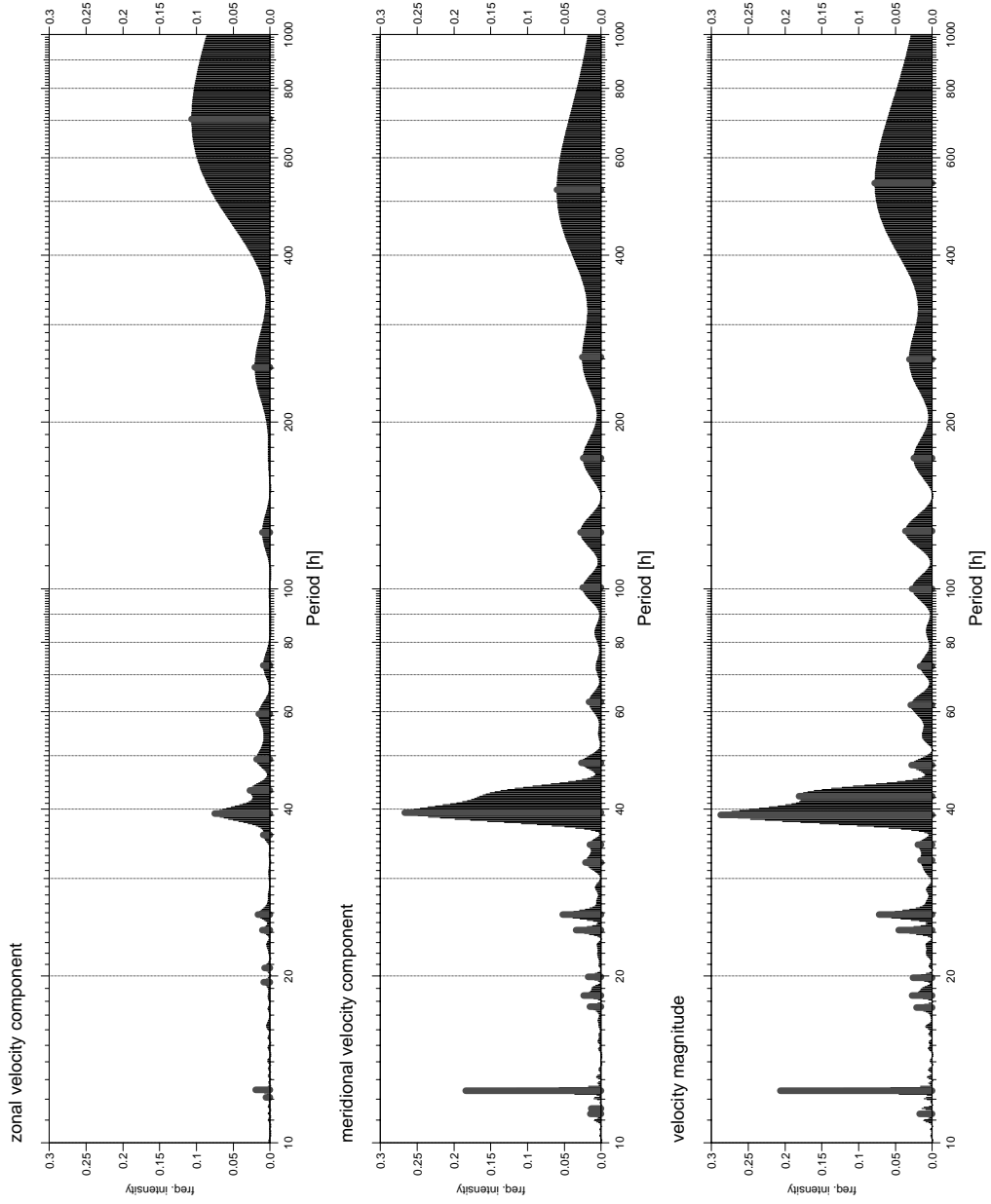


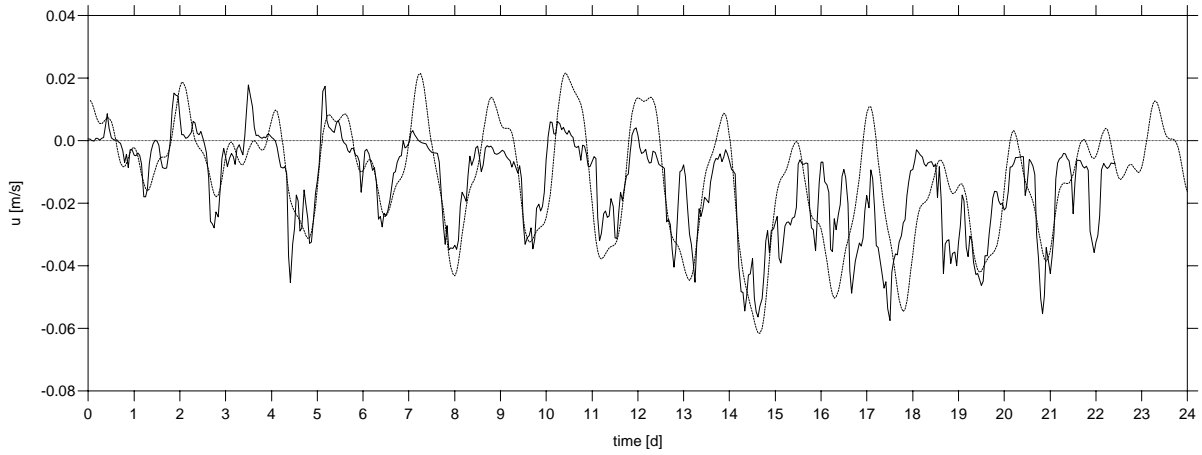
Fig. 3. Stick plot of available current measurements (rough data from NOAA BIE).



NOAA21, 23d, 2mab

Fig. 4. Periodogramme of the currents measured by the NOAA 21 mooring for 23 days (2 m above bottom).

NOAA 21, zonal velocity component u



NOAA 21, meridional velocity component v

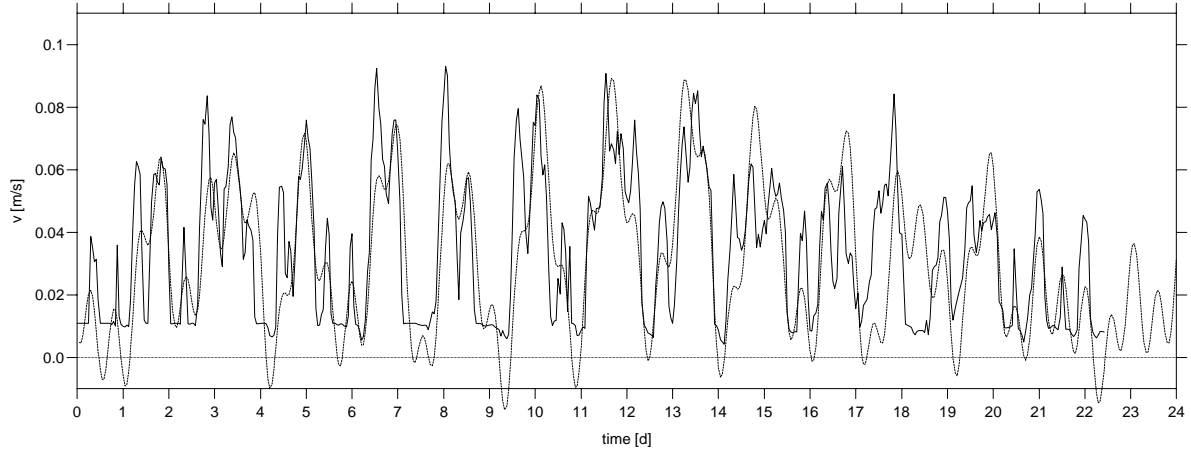


Fig. 5. Comparison: measured current velocity and approximate current velocity.

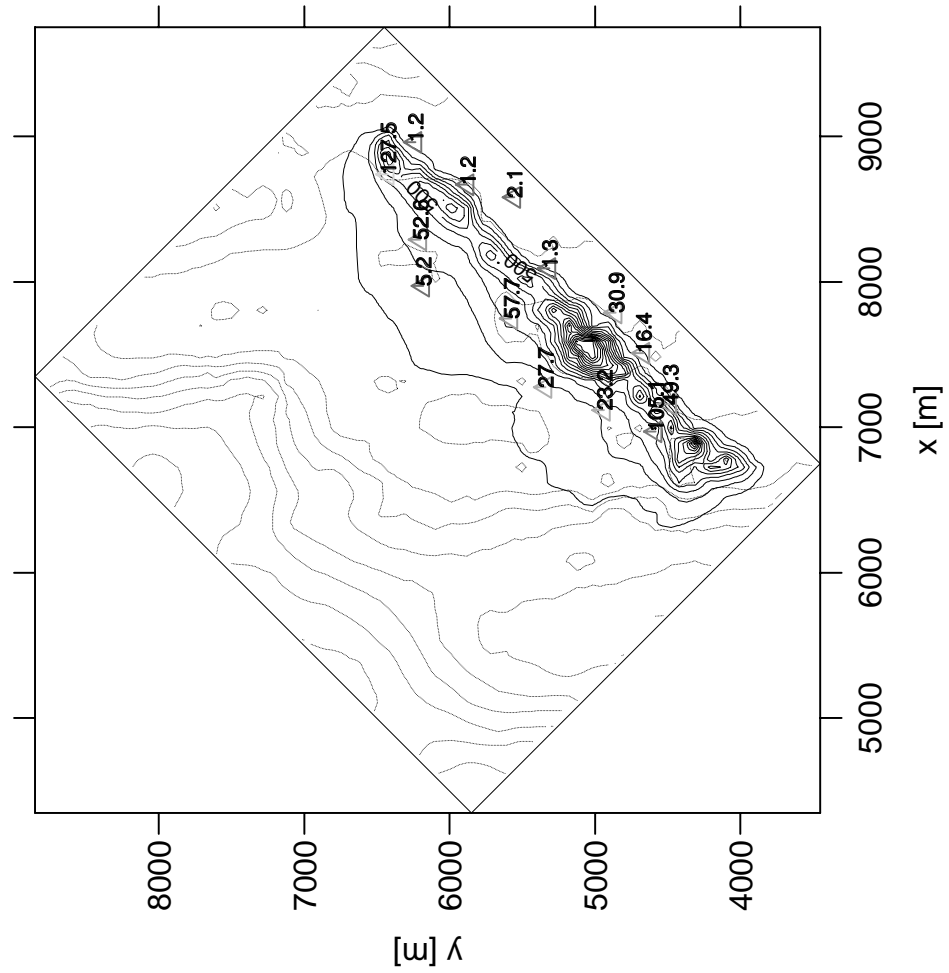


Fig. 6. The final sediment deposition caused by the NOAA BIE discharges. Deposition range 100-2000g/m², isoline step 100g/m². Depositions measured in sediment traps (triangles, 2 mab) given in the same units.

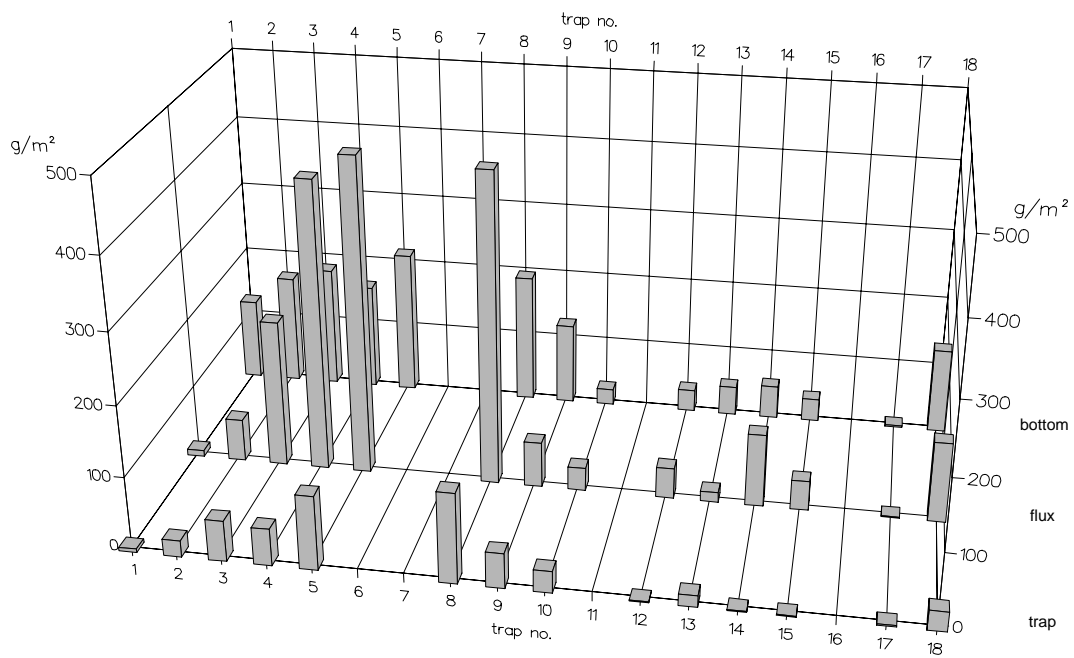


Fig. 8. BIE model, the sediment deposition in traps compared with computed values at the bottom and at the level of 2 mab.

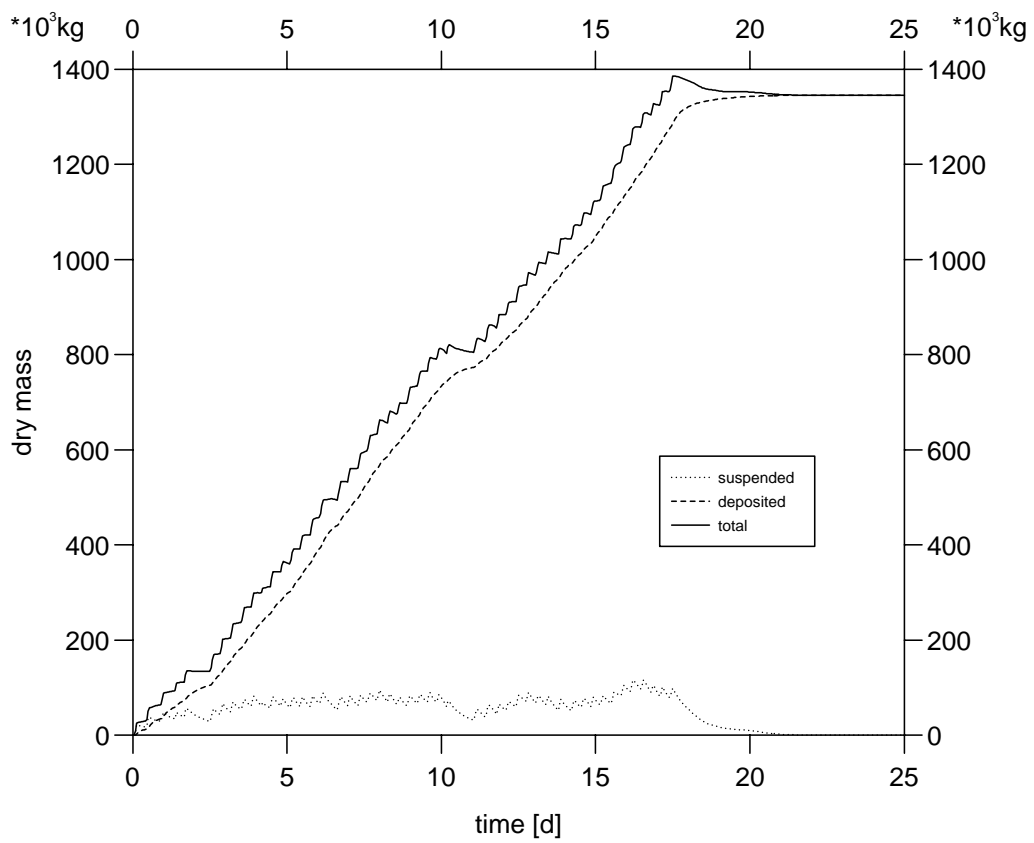


Fig. 9. BIE model, resuspended sediment mass balance.

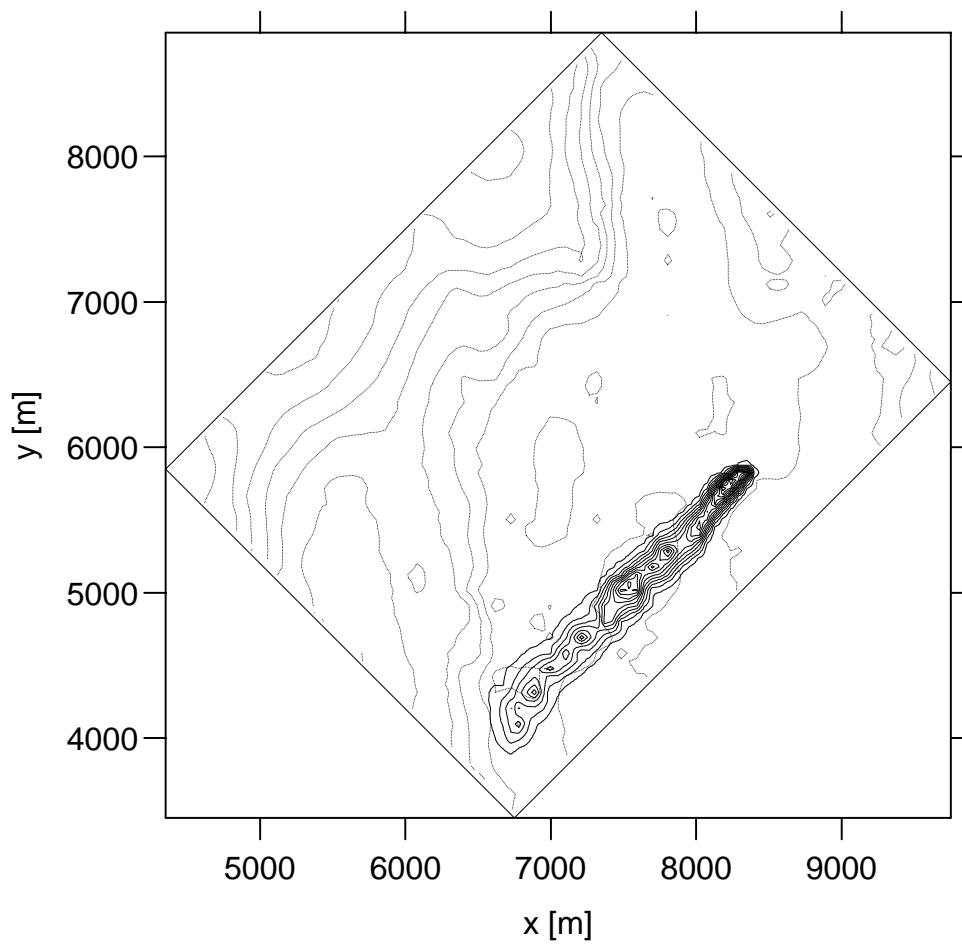


Fig. 10. An example of plume during the emission (first tow). Concentration at the bottom level. Iso-lines each 2 mg/l, maximum value 30 mg/l.

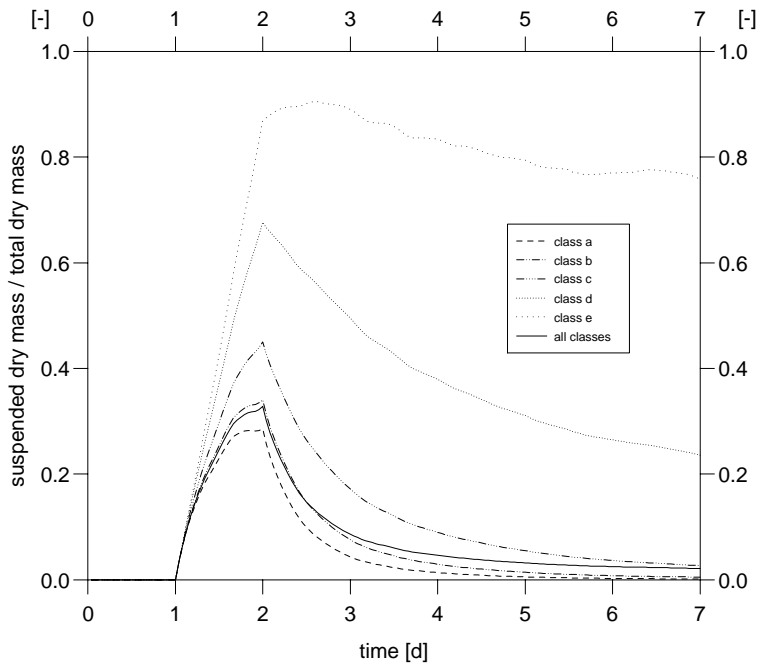


Fig. 11. Mass balances for suspended (dry) sediment mass relative to total emitted (dry) mass in a given settling velocity class, look Table 3.

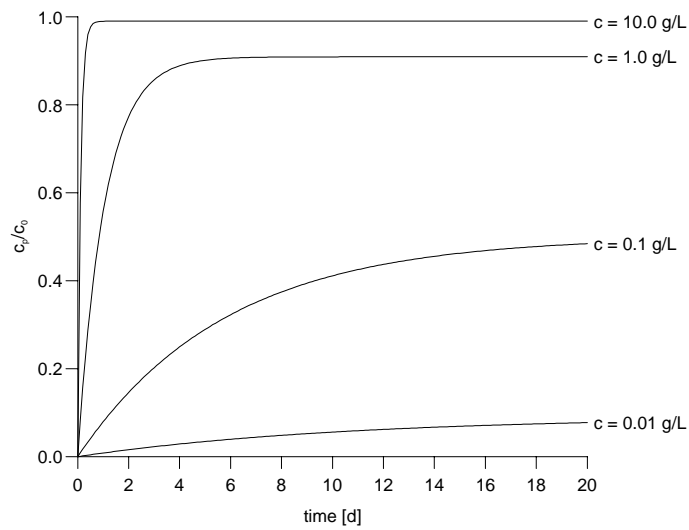


Fig. 12. Examples of one-stage sorption processes in a closed system for various constant sediment concentrations c . Initially $c_d = c_0$, $c_p = 0$. Only sorbed concentrations are shown. The values of process rates are: $k_1 = k_2 K c$, $k_2 = 10^{-6} \text{ s}^{-1} = 0.0864 \text{ d}^{-1}$, $K = 10 \text{ m}^3/\text{kg}$.

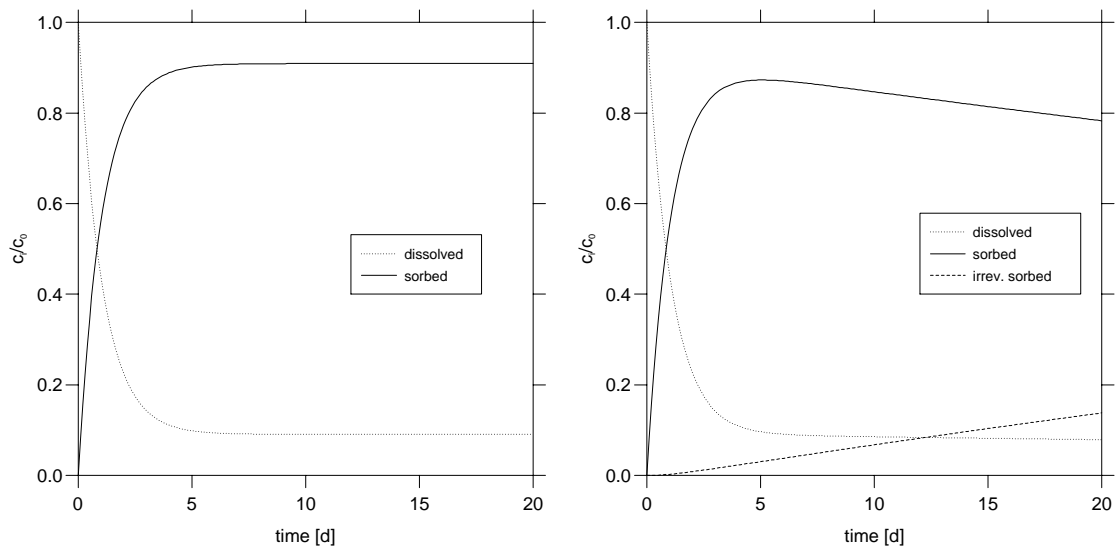


Fig. 13. Examples of the one-stage (left) and the two-stage (right) sorption in a closed system for constant sediment concentration. Initially $c_d = c_0$, $c_p = 0$, $c_l = 0$. The values of process rates are: $k_1 = 10^{-5} \text{ s}^{-1} = 0.864 \text{ d}^{-1}$, $k_2 = 10^{-6} \text{ s}^{-1} = 0.0864 \text{ d}^{-1}$, $k_3 = 10^{-7} \text{ s}^{-1} = 0.00864 \text{ d}^{-1}$.

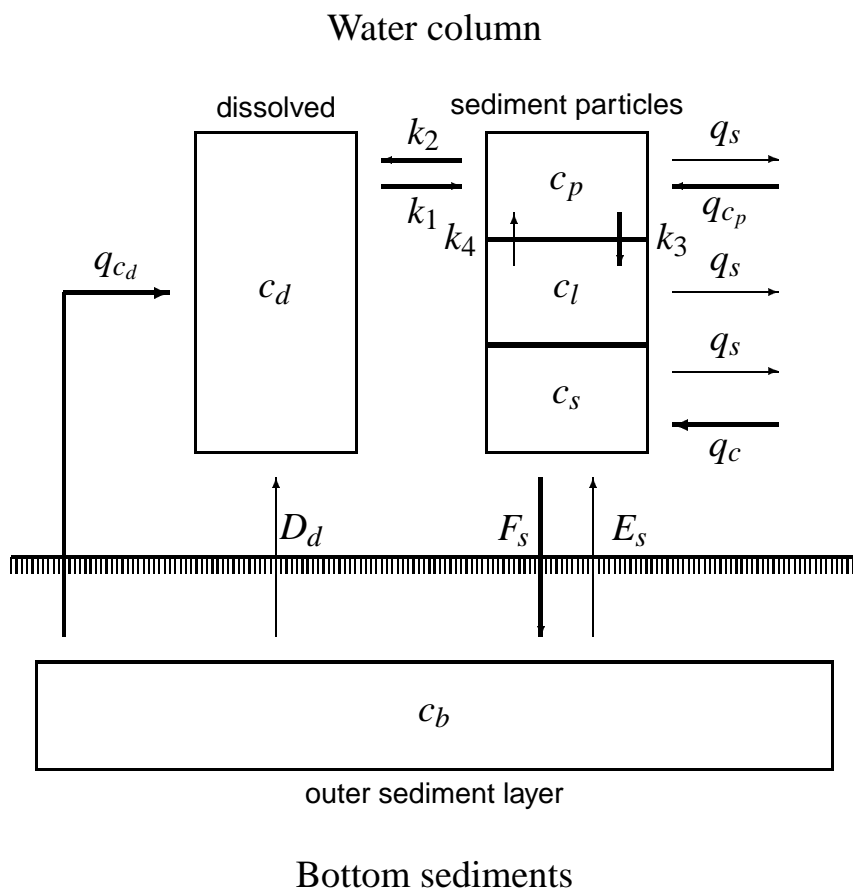


Fig. 14. A metal cycling model. Concentrations: c_s suspended sediment, c_d dissolved metal, c_p bounded (reversibly sorbed) metal, c_l (almost) irreversibly bounded metal; c_b metal dissolved in interstitial water; fluxes: F_s settling of sediment particles, E_s sediment erosion, D_d diffusion of dissolved metal. Source terms: q_c discharged sediment, q_{cd} discharged dissolved metal, q_{cp} discharged metal in the particulate phase, q_s scavenging by external, ambient particles. k_i : sorption/resorption rates, explained in text. Thick lines: implemented processes, thin lines: neglected processes.

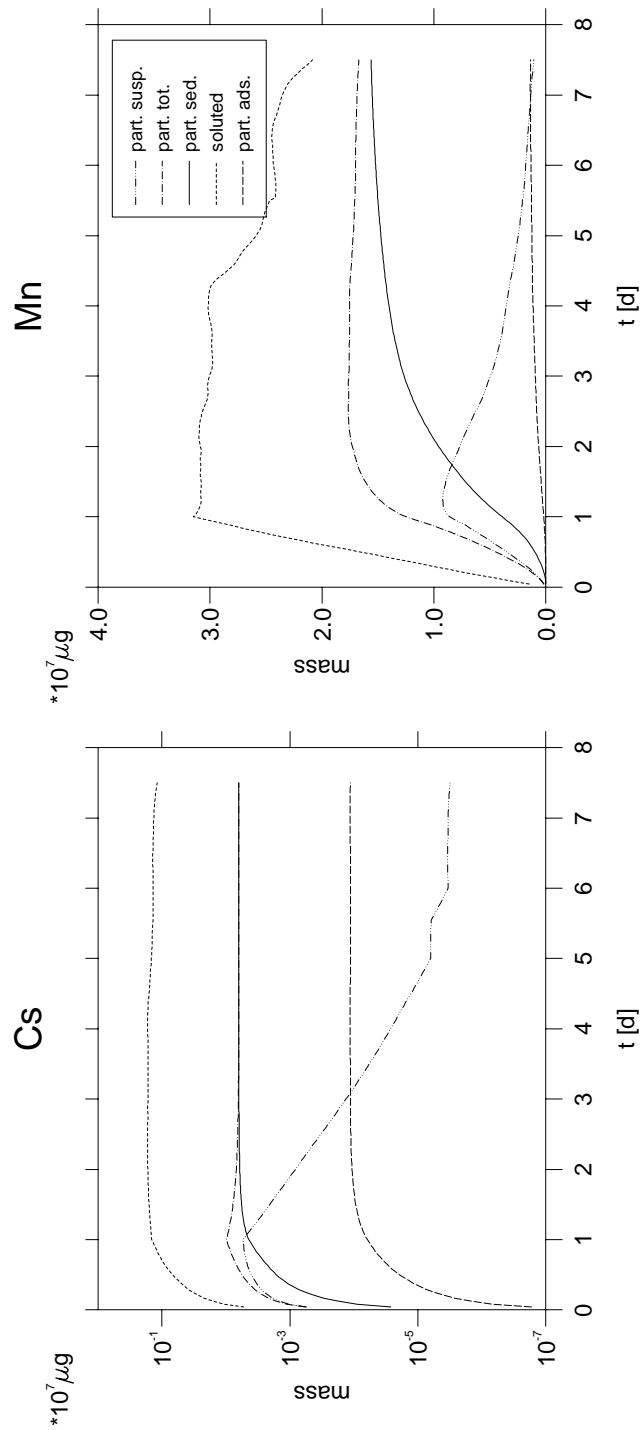


Fig. 15. Mass balance for *Cs* and *Mn* when discharged for a period of 1 day. Abbreviations: *part.* in particulate phase, *susp.* in suspension, *tot.* total, *sed.* deposited, *ads.* irreversibly adsorbed (in suspension).

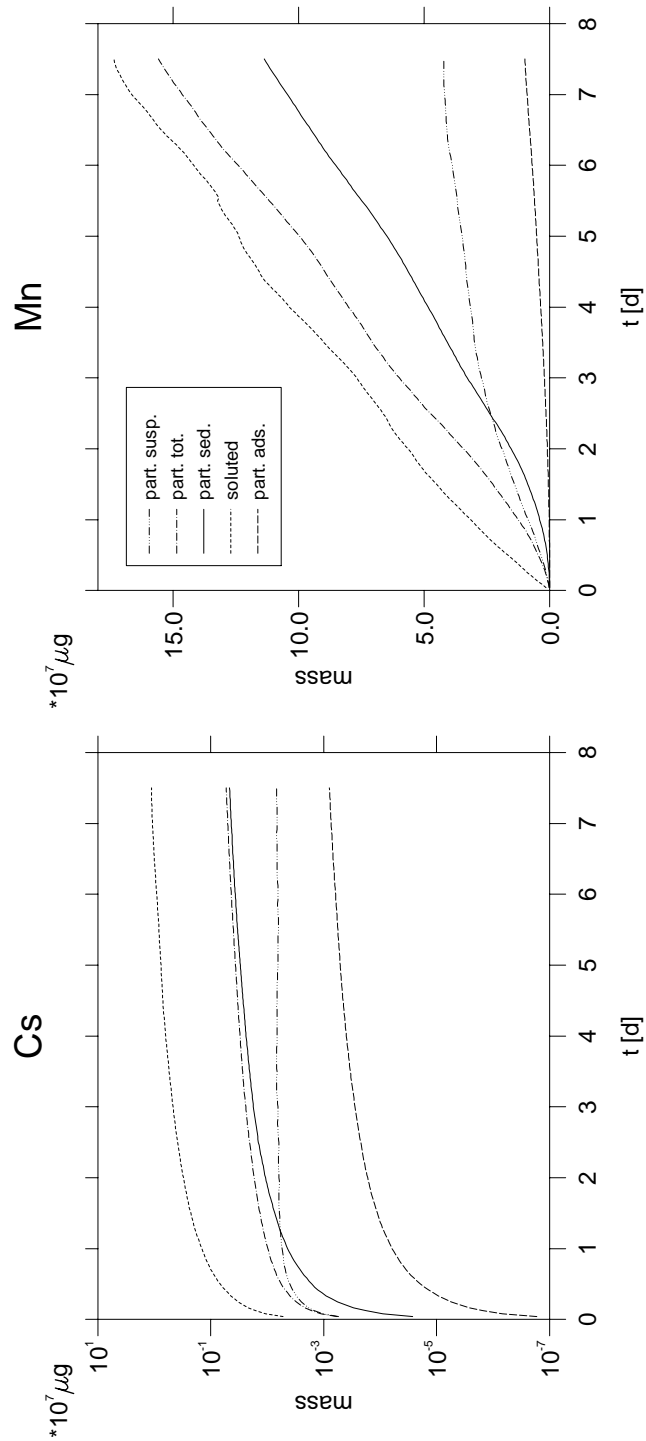


Fig. 16. Mass balance for *Cs* and *Mn* when discharged continuously for 7 days. Abbreviations: *part.* - in particulate phase, *susp.* in suspension, *tot.* total, *sed.* deposited, *ads.* irreversibly adsorbed (in suspension).

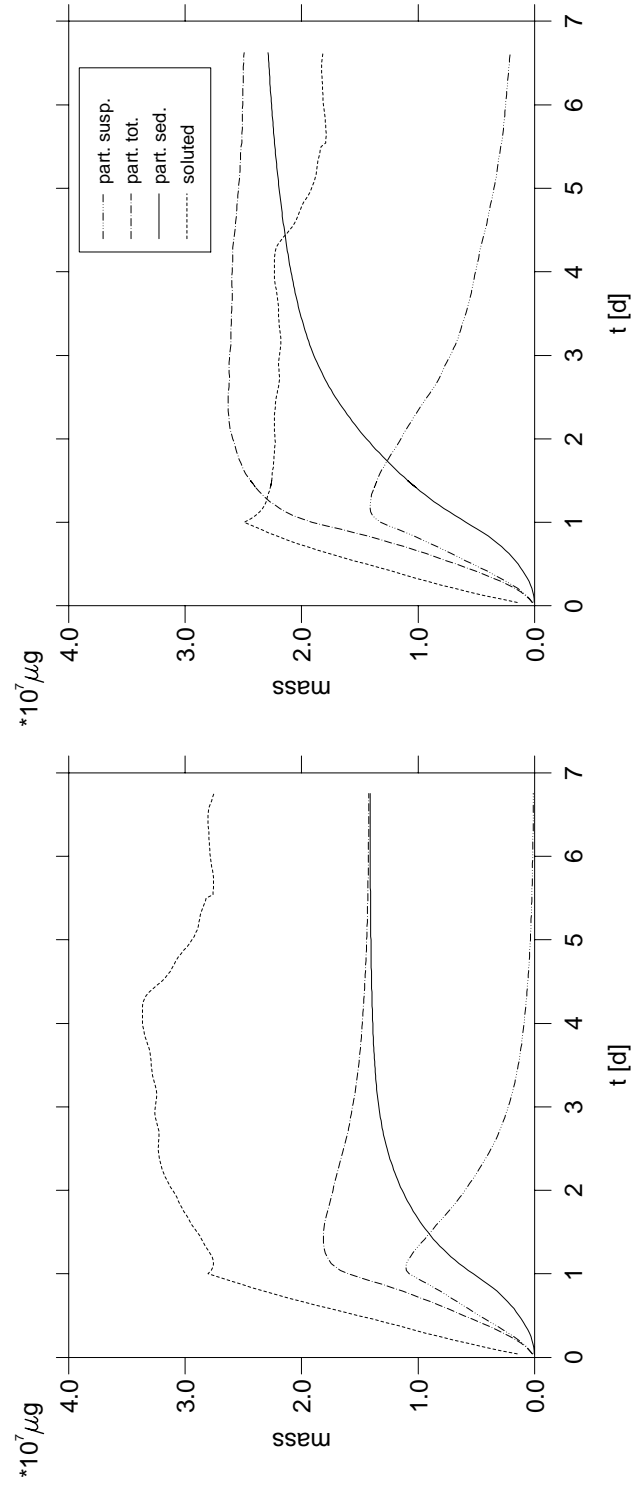


Fig. 17. Mass balance for two hypothetical metals. Left: $k_2 = 1.0 \cdot 10^{-5} \text{ s}^{-1}$, $K = 100 \text{ m}^3 \text{ kg}^{-1}$. Right: $k_2 = 1.0 \cdot 10^{-6} \text{ s}^{-1}$, $K = 1000 \text{ m}^3 \text{ kg}^{-1}$. In both cases $k_3 = 0$. Abbreviations: *part.* in particulate phase, *susp.* in suspension, *tot.* total, *sed.* sedimented (deposited).

Table 1

DISCOL sediment classes and their settling velocities

Class	d_i μm	$\Delta\rho$ kg/m^3	w_{si} m/s	$n(d_i)$	$nm(d_i)$
a	100	76.7	$2.41 \cdot 10^{-4}$	0.14	0.7933
b	80	102.5	$2.06 \cdot 10^{-4}$	0.03	0.0890
c	50	192.2	$1.51 \cdot 10^{-4}$	0.07	0.0547
d	30	238.2	$6.74 \cdot 10^{-5}$	0.36	0.0630
e	3	626.5	$1.77 \cdot 10^{-6}$	0.40	0.0001

Table 2

Assumed track extreme points.

Point	Latitude	Longitude	x [m]	y [m]
Start	12 55.20	-128 36.30	6683.5	4076.6
End	12 56.50	-128 35.05	8939.8	6485.5
Track length 3300 m				

Table 3

BIE Settling velocity distribution for concentration 15 mg/l.

Range [m/s]	Fractional percentage
$10^{-7} - 10^{-6}$	30 %
$10^{-6} - 10^{-5}$	15 %
$10^{-5} - 10^{-4}$	35 %
$10^{-4} - 10^{-3}$	20 %
Mean settling velocity 1.2×10^{-4} m/s	

Table 4
BIE sediment trap contents.

Trap Nr	x [m]	y [m]	z GPS [m]	z [m]	m_{dep} (trap) [g/m ²]	m_{dep} (bottom) [g/m ²]	m_{dep} (2mab) [g/m ²]
1	7971.	6182.	-4842.	-4878.	118.6	9.0	5.2
2	7118.	4936.	-4843.	-4876.	159.9	61.0	23.2
3	7748.	5574.	-4851.	-4881.	177.6	211.6	57.7
4	8290.	6202.	-4860.	-4879.	155.1	417.7	52.6
5	6969.	4582.	-4858.	-4878.	209.7	453.8	105.1
8	8738.	6424.	-4859.	-4870.	188.4	445.8	127.5
9	7156.	4482.	-4846.	-4879.	118.7	65.1	49.3
10	7788.	4857.	-4906.	-4879.	22.8	33.1	30.9
12	8960.	6235.	-4858.	-4865.	31.6	44.1	1.2
13	7510.	4668.	-4870.	-4881.	42.4	14.2	16.4
14	8094.	5313.	-4837.	-4874.	48.1	104.6	1.3
15	8667.	5876.	-4833.	-4870.	33.2	42.6	1.2
17	8580.	5555.	-4864.	-4867.	2.3	1.6	2.1
18	7274.	5340.	-4842.	-4876.	123.7	115.4	27.7

Table 5
Current characteristics (NOAA 21).

Number of measurements n	3304
Time interval Δt	600.0 s
Mean zonal velocity \bar{u}	-0.0147 m/s
Variability range u_{min}, u_{max}	-0.0779, 0.0218 m/s
Mean meridional velocity \bar{v}	0.0341 m/s
Variability range v_{min}, v_{max}	-0.0139, 0.1010 m/s
Mean scalar velocity \bar{v}_{scal}	0.0394 m/s
Maximal scalar velocity $v_{scalmax}$	0.1070 m/s
Minimal scalar velocity $v_{scalmin}$	0.0000 m/s
Mean vector velocity \bar{v}_{vect}	0.0371 m/s
Stability factor SF	0.9423
Mean direction $\varphi(\bar{u}, \bar{v})$	336.7°

Table 6
Current scenario components.

Nr	Period [h]	Comment
1	41.0	inertial
2	39.4	inertial
3	37.5	inertial
4	12.42	M2 principal lunar semidiurnal tide
5	25.82	O1 principal lunar diurnal tide
6	23.93	K1 luni-solar diurnal tide

Table 7
Mass balance for BIE modeling.

Days	Emission [kg]	Mass [kg] in water column
0-5	326797	64313
5-10	454171	78535
10-15	376187	73965
15-20	241360	9384
20-25	0	0.48
Σ	1398515	

Table 8
Two-stage sorption coefficients

Metal	k_2	k_3	K
<i>Mn</i>	0.018 d ⁻¹	0.048 d ⁻¹	2200 m ³ kg ⁻¹
	$2.08 \cdot 10^{-7}$ s ⁻¹	$5.55 \cdot 10^{-7}$ s ⁻¹	
<i>Co</i>	0.011 d ⁻¹	0.013 d ⁻¹	2200 m ³ kg ⁻¹
	$1.27 \cdot 10^{-7}$ s ⁻¹	$1.5 \cdot 10^{-7}$ s ⁻¹	
<i>Cs</i>	1.5 d ⁻¹	0.016 d ⁻¹	0.4 m ³ kg ⁻¹
	$1.74 \cdot 10^{-5}$ s ⁻¹	$1.85 \cdot 10^{-7}$ s ⁻¹	